Received: 30 December 2024 | Revised: 19 April 2026 | Accepted: 15 June 2026

DOI: 10.33012/navi.791

ORIGINAL ARTICLE

A Recursive Bayesian Overbounding Filter Using Gaussian–Pareto Distributions

Yingjie Hu* | **Demoz Gebre-Egziabher**

[1] Department of Aerospace Engineering and Mechanics, University of Minnesota, Twin Cities, Minnesota, USA

Correspondence
*Yingjie Hu
Email: hu000258@umn.edu

Abstract

We introduce a recursive estimator for positioning, navigation, and timing (PNT) systems that ensures bounded tail probabilities for system output errors. This estimator leverages Gaussian–Pareto distributions and the Dvoretzky–Kiefer–Wolfowitz inequality to provide conservative overbounds for sensor noise constructed from finite data. To enable efficient propagation of Gaussian–Pareto distributions, we develop a method that employs Gaussian mixture models to conservatively approximate these distributions. Given that convolutions with Gaussian mixtures can result in exponential growth of the mixture terms, we devise a culling algorithm that periodically prunes the Gaussian mixture while ensuring conservative overbounding. We assess the performance of the recursive algorithm using a linear, one-dimensional PNT problem. Simulation results consistently demonstrate that the protection levels computed using the proposed algorithm are smaller than those obtained through the traditional Gaussian overbounding method. These results highlight the potential of the proposed estimator to improve PNT system availability in safety-critical applications.

Keywords

Bayesian inference, Gaussian–Pareto, GMM, integrity, overbounding

1 | INTRODUCTION

Integrity is a critical measure of a positioning, navigation, and timing (PNT) system's ability to promptly and accurately alert users when the system's performance deteriorates to a level that poses a potential risk. Integrity is especially important for safety-critical PNT systems, where undetected errors could lead to severe consequences, including potential loss of life, significant property or environmental damage, etc. Integrity risk quantifies the probability of an occurrence of an undetected navigation error or failure that can cause hazardous consequences.

To better understand the concept of integrity, let us consider the scenario shown in Figure 1, which depicts autonomous ground vehicles traveling on a two-lane highway. The PNT systems onboard supply position estimates for each vehicle, whose errors are random variables with some probability distribution. If we have perfect knowledge of the uncertainty of the PNT systems, we can calculate the probability density function (PDF) of the true position error (red). Although the majority of the PDF mass is centered in the middle of the lane, there is a small but

Licensed under CC-BY 4.0 © 2026 Institute of Navigation

finite probability in the tails (purple area), indicating that the vehicle could either collide with oncoming traffic or run off of the road. If the PNT system fails to alert the user to a potential risk when the position error exceeds a predefined alert limit, this event is referred to as a *misleading information* event (Walter et al., 1999). When the associated failure consequences fall within the hazardous classification, these events are further categorized as *hazardously misleading information* (*HMI*) events (Blanch et al., 2012; European Space Agency, 2025; Zhai et al., 2019). The probability of *HMI* events must be precisely known and bounded during the certification process of safety-critical PNT systems. For instance, the Federal Aviation Administration requires that safety-critical PNT systems, particularly those used in aviation, maintain extremely low integrity risk, with acceptable probabilities depending on the severity classification of the associated failure condition (Federal Aviation Administration, 2023). Typical requirements are on the order of 1×10^{-7} for hazardous conditions and 1×10^{-9} for catastrophic conditions (Federal Aviation Administration, 2024).

Precise quantification of the probability of *HMI* events corresponds to the problem of estimating tail probabilities. In practice, however, our knowledge of the system uncertainty is often limited, making accurate tail probability estimation challenging. Accurately quantifying tail probabilities to the levels of safety requirements often demands large amounts of data, and the collection of such extensive data sets can be a lengthy process, potentially spanning years, which can greatly delay the certification process for safety-critical PNT systems.

To address this issue, a conservative distribution of the estimated position error (as shown by the blue curve in Figure 1) can be constructed based on a limited amount of data. The conservative distribution is then used in lieu of the unknown true error distribution. Based on this conservative distribution, a protection level is computed. The protection level is a statistical bound on the position error that is designed to bound the true (unknown) position error with a specified probability determined by the integrity requirement. During operation, the protection level is compared against a predefined alert limit, which represents the maximum allowable error to maintain safe operation. If the protection level exceeds the alert limit, the navigation system is declared unavailable, and an alarm is raised to warn the user.

This conservative PDF approach offers two key benefits. First, it can potentially shorten the certification process by limiting the amount of data collection needed

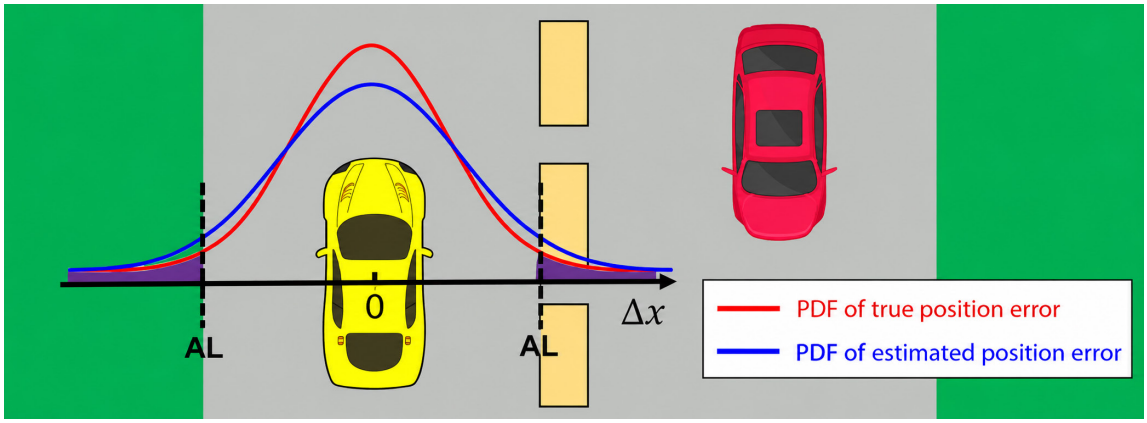

FIGURE 1 Diagram of vehicles on a two-lane highway
The PDF of the estimated position error (blue) is an overbound of the PDF of the true position error (red). AL: alert limit

(Larson & Gebre-Egziabher, 2017; Larson, 2018). Second, by maintaining bounded tail probabilities of *HMI* events, the conservative PDF ensures that the calculated protection level consistently bounds the true position error (DeCleene, 2000; Wang et al., 2020), enhancing safety by effectively managing extreme error risks. The technique of developing conservative distributions to bound the tail probabilities is known as overbounding.

1.1 | Overbounding

DeCleene (2000) developed a definition of overbounding based on the cumulative distribution function (CDF), which can be expressed as follows:

$$\begin{aligned} F_O(x) &\geq F(x) \quad \forall x \in \{x \mid F(x) \leq 0.5\} \\ F_O(x) &\leq F(x) \quad \forall x \in \{x \mid F(x) \geq 0.5\} \end{aligned} \tag{1}$$

If the two CDFs $F_O(x)$ and $F(x)$ satisfy the relationship described in Equation (1), $F_O(x)$ is defined as an overbound to $F(x)$. DeCleene (2000) demonstrated that the linear combination of multiple error sources is overbounded, provided that each contributing error component is overbounded. This property holds as long as the distributions of error components and the overbounds are zero-mean, symmetric, and unimodal. However, this requirement limits the acceptable distribution shapes for the single-CDF overbound theorem. Rife et al. (2006) proposed the paired overbounding approach, which has been proven to hold through convolution by maintaining a pair of left and right tail bounds. Unlike single-CDF overbounding, the paired overbounding method accommodates error distributions of arbitrary shapes, making it more versatile for complex error distributions. A two-step Gaussian overbounding method proposed by Blanch et al. (2018) combines single-CDF overbounding and paired overbounding, which can overcome the main limitations of the previous techniques. Additionally, when correlation exists among individual error sources, the symmetric overbounding algorithm developed by Rife and Gebre-Egziabher (2007) can be used by leveraging a linear mapping to decorrelate the sources. These approaches typically utilize a Gaussian distribution as the overbounding model of choice owing to its extensive application in modeling uncertainties in PNT problems and its beneficial property that the convolution of multiple Gaussian distributions remains Gaussian. However, in practice, error distributions with non-Gaussian, heavy-tailed characteristics are often encountered. We refer to distributions whose tail probabilities decay at least exponentially with increasing error magnitude, as is the case for Gaussian and other sub-Gaussian distributions, as "exponentially bounded." In contrast, heavy-tailed distributions, such as Student's t distributions with low degrees of freedom, exhibit polynomial tail decay and are therefore not exponentially bounded. Gaussian-based overbounding approaches fail to tightly overbound such heavy tails. To conservatively bound these non-exponentially bounded tails, the variance of a Gaussian overbound must be excessively inflated, resulting in an overly conservative model that can significantly reduce the availability of PNT systems (Rife & Pervan, 2012; Rife et al., 2004). Here, *availability* refers to the fraction of time during which the navigation system can provide a valid solution while satisfying integrity requirements; overly conservative overbounds inflate protection levels, increasing the likelihood that they will exceed alert limits and thereby causing the system to be declared unavailable when the true position error remains acceptable.

To address the limitation of Gaussian-based overbounding in modeling heavy-tailed distributions, Rife et al. (2004) developed the core overbounding technique for error distributions with heavier-than-Gaussian tails by decomposing the bound into the core and tail parts. Blanch et al. (2008) used a bimodal Gaussian mixture model (GMM) to account for the tight core and heavy tails of the error distribution. Yan et al. (2024) proposed the principal Gaussian overbounding approach to overbound the CDF of the bimodal GMM, which is employed to fit the underlying heavy-tailed error distribution. However, these approaches rely on data samples to establish overbounding models.

Capturing the far tails of actual error distributions generally demands substantial data collection, which can extend the time required for the certification process significantly. Similar to the core and tail partition presented by Rife et al. (2004), Larson et al. (2019a) proposed a Gaussian–Pareto overbounding approach by modeling the core of the actual error distribution by a Gaussian and tails by generalized Pareto distributions (GPDs). This method can achieve tight overbounds for heavy tails of an error distribution with a limited amount of data, potentially accelerating the process of conservatively estimating the tail probabilities and increasing the availability of PNT systems. In this paper, we will leverage the Gaussian–Pareto overbound to design a PNT filter that can maintain bounded tail probabilities.

1.2 | Overview of the Gaussian–Pareto Approach

The Gaussian–Pareto overbounding approach is grounded in extreme value theory (EVT), a statistical tool that indicates that the tail portion of any distribution can be asymptotically approximated by a GPD (Pickands, 1975). The conditional excess distribution function (CEDF) can be used to model the tails of a distribution. For instance, the CEDF of the right tail can be expressed as follows:

$$F_{\text{CEDF}}(x) = \frac{F(u+x) - F(u)}{1 - F(u)} \quad \text{for} \quad 0 \le x \le x_F - u \tag{2}$$

where $x_F = \sup(x : F(x) < 1)$ denotes the right endpoint of the support of $F(x)$. u is the point at which the right tail portion begins. The EVT states that we have the following for some real-valued number γ:

$$\lim_{u \to x_F} \inf_{0<\beta<\infty} \sup_{0 \le x < \infty} |F_{\text{CEDF}}(x) - G(x; \gamma, \beta)| = 0 \tag{3}$$

where $G(x; \gamma, \beta)$ is the CDF of the GPD, characterized by the shape parameter γ and scale parameter β. The CDF equation of the GPD can be expressed as follows:

$$G(x; \gamma, \beta) = \begin{cases} 1, & \gamma < 0, x > -\frac{\beta}{\gamma} \\ 1 - e^{-\frac{x}{\beta}}, & \gamma = 0 \\ 1 - \left(1 + \frac{\gamma}{\beta} x\right)^{-\frac{1}{\gamma}}, & \text{otherwise} \end{cases} \tag{4}$$

The GPD parameters γ and β can be estimated via the maximum likelihood estimator (MLE) using data sampled from the tail region. For example, the MATLAB function `gpfit` can be used to calculate the maximum likelihood estimates of these two parameters.

A conservatism assessment of the estimated GPD for heavy tails was performed by Larson and Gebre-Egziabher (2017). It was demonstrated that a conservative GPD can be obtained by increasing the shape and scale parameters, i.e., $G(x;\gamma+\Delta\gamma,\beta+\Delta\beta)\le G(x;\gamma,\beta)$ for $\forall\Delta\gamma\ge 0,\forall\Delta\beta\ge 0$. Thus, the conservative GPDs are adopted as overbounding models for both tails. Moreover, careful adjustment of increased $\Delta\gamma$ and $\Delta\beta$ is required to account for estimation and modeling errors.

Assuming that the random variable X has a distribution that is zero-mean and heavy-tailed, the CDF of the Gaussian–Pareto overbound $F_{\text{G-P}}(x)$ can be expressed as follows:

$$F_{\text{G-P}}(x)=\begin{cases}F_{\text{Gauss}}\left(u_{\text{L}}\right)-G_{\text{L}}\left(u_{\text{L}}-x;\gamma_{\text{L}},\beta_{\text{L}}\right)F_{\text{Gauss}}\left(u_{\text{L}}\right), & x\le u_{\text{L}}\\ F_{\text{Gauss}}(x), & u_{\text{L}}<x\le u_{\text{R}}\\ G_{\text{R}}\left(x-u_{\text{R}};\gamma_{\text{R}},\beta_{\text{R}}\right)\left(1-F_{\text{Gauss}}\left(u_{\text{R}}\right)\right)+F_{\text{Gauss}}\left(u_{\text{R}}\right), & x>u_{\text{R}}\end{cases} \tag{5}$$

where u_{L} and u_{R} denote the thresholds for the left-hand and right-hand tails. F_{Gauss} represents the Gaussian overbounds of the core of the underlying distribution. $G_{\text{L}}(x;\gamma_{\text{L}},\beta_{\text{L}})$and $G_{\text{R}}(x;\gamma_{\text{R}},\beta_{\text{R}})$are the CDFs of the GPD with the adjusted overbounding parameters γ and β for the left-hand and right-hand tails. Readers are referred to the works by Larson and Gebre-Egziabher (2017) and Larson et al. (2019a) for more details on the Gaussian–Pareto overbounds.

The Gaussian–Pareto overbounding approach has the advantage of producing tight overbounds for heavy tails using a limited amount of data. However, because the true underlying distribution remains unknown and the estimated GPD is only an approximation of the tail distribution, the overbounding parameter adjustment approach reported by Larson and Gebre-Egziabher (2017) is empirical. Thus, a systematic assessment of how well this approach conservatively overbounds the true distribution is still lacking. Moreover, Larson et al. (2019a) only assessed Gaussian–Pareto overbounds in the range domain. Unlike Gaussian distributions, Gaussian–Pareto distributions do not have clear convolution properties, which restricts their use in PNT filtering frameworks. Consequently, there still remains a need for a PNT algorithm capable of propagating Gaussian–Pareto distributions to reliably provide conservative overbounds of system output errors.

1.3 | Problem Statement

Given the variety and complexity of modern multi-sensor PNT systems, a typical way of constructing overbounds on the PNT system output errors is to develop overbounds of the input errors and then propagate the input overbounds through a navigation filter/estimator to obtain overbounds on the system output errors (Larson et al., 2019a). This input–output overbounding relationship is illus-trated in Figure 2. The Gaussian–Pareto overbounding approach has demonstrated potential in tightly overbounding unknown heavy-tailed distributions with limited data, offering a promising avenue to expedite the certification process and increase the availability of safety-critical PNT systems. However, a key challenge remains: Gaussian–Pareto distributions do not preserve their form through convolution, complicating their integration into PNT system design. Therefore, this paper addresses the following research question: *How can Gaussian–Pareto overbounds be effectively propagated through PNT estimators/filters?* We propose a solution to this question in the form of a recursive estimator that makes use of the GMM concept to achieve a

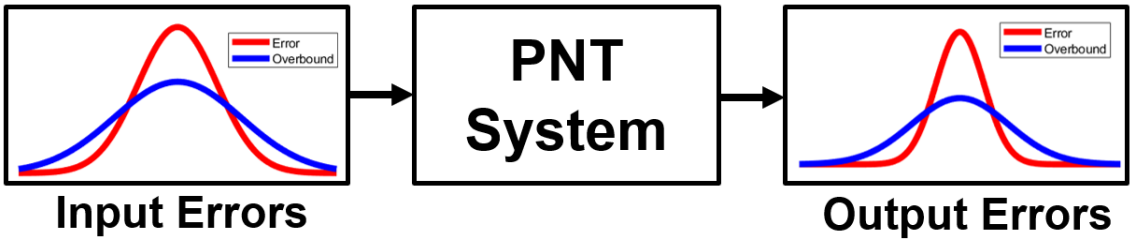

FIGURE 2 Flow chart of the input–output overbounding relationship for a generic PNT system
The input to the PNT system is the sensor measurements, and the output is the PNT state estimates.

mathematically tractable formulation of a Bayesian estimator that accurately and efficiently propagates Gaussian–Pareto overbounds.

1.4 | Paper Organization and Contribution

Based on work originally presented by Hu (2024), this paper focuses on designing a recursive PNT filter for safety-critical applications that can take Gaussian–Pareto overbounds as input and ensure bounded tail probabilities for the system output errors. This paper's contributions are threefold. First, we propose a systematic approach for determining the relevant parameters of Gaussian–Pareto overbounds based on a statistical tool called the Dvoretzky–Kiefer–Wolfowitz (DKW) inequality. This approach accounts for uncertainty in the empirical CDF obtained from finite sample data and allows for a quantifiable measure of confidence in overbounding the true, typically unknown, underlying distribution. Second, we propose a nonlinear least-square-based GMM estimation approach to conservatively approximate the Gaussian–Pareto distribution by a GMM, which retains both the fidelity of the Gaussian–Pareto distribution and the useful convolutional properties of Gaussian distributions. Third, we design a GMM-based recursive Bayesian overbounding filter to propagate the Gaussian–Pareto overbounds. To address the issue of exponential growth in the number of Gaussian mixture terms caused by density convolution, we propose a culling algorithm that periodically prunes the Gaussian mixture components while ensuring conservative overbounding.

The proposed recursive Bayesian overbounding filter is outlined using the pseudocode listed in Algorithm 1. The organization of this paper follows the order of the pseudocode. First, Section 2 focuses on developing Gaussian–Pareto overbounds of the unknown sensor errors based on the DKW inequality (lines 1–2). We obtain a quantitative assessment of confidence in overbounding the true underlying distribution. In Section 3, in order to utilize the Gaussian–Pareto overbound in a PNT filter, we propose a least-square-based GMM estimation approach to approximate the Gaussian–Pareto distribution with a GMM (lines 3–4). Overbounding constraints are introduced to ensure that conservatism is preserved in this process. Next, in Section 4, by leveraging Bayesian inference, we present the equations of a recursive Bayesian overbounding filter that can take as input the conservative GMM overbound as a sensor noise model and that outputs estimates of the PNT states (lines 5–18). A simulation case study is implemented in Section 5 to validate the efficacy of the proposed methodology. A discussion of the utility and significance of this work is presented in Section 6. We close the paper with a conclusion and possible directions for future work.

ALGORITHM 1
Recursive Bayesian Overbounding Filter

INPUT: Unknown, non-Gaussian, heavy-tailed sensor error $\mathbf{v}_t$
OUTPUT: Overbound distribution of the system output error

Collect data from the sensor noise distribution
Develop the Gaussian–Pareto distribution $\mathbf{v}_{G\text{-}P}$ to overbound $\mathbf{v}_t$ based on the DKW inequality
Estimate the conservative GMM $\mathbf{v}_{GMM}$ that best fits $\mathbf{v}_{G\text{-}P}$ using Equation (13)
Use GMM $\mathbf{v}_{GMM}$ to overbound $\mathbf{v}_t : \mathbf{v}_t \leftarrow \mathbf{v}_{GMM}$
while ($k \leq$ Maximum time steps) **do**
    Update the *a priori* PDF $\mathbf{P}(\mathbf{x}_k|\mathbf{Y}_{k-1})$ using Equation (21)
    if $\mathbf{y}_k$ is available **then**
        if first measurement update **then**
            Update *a posteriori* PDF $\mathbf{P}(\mathbf{x}_k|\mathbf{Y}_k)$ using Equation (23)
        else
            Update *a posteriori* PDF $\mathbf{P}(\mathbf{x}_k|\mathbf{Y}_k)$ using Equation (26)
        end if
    end if
    if Gaussian mixture terms of $\mathbf{P}(\mathbf{x}_k|\mathbf{Y}_k) \geq$ threshold **then**
        Fit a new GMM $\mathbf{P}_{GMM}(\mathbf{x}_k|\mathbf{Y}_k)$ with fewer terms to $\mathbf{P}(\mathbf{x}_k|\mathbf{Y}_k)$ using Equation (13)
        $\mathbf{P}(\mathbf{x}_k|\mathbf{Y}_k) \leftarrow \mathbf{P}_{GMM}(\mathbf{x}_k|\mathbf{Y}_k)$
    end if
end while

2 | OVERBOUND DEVELOPMENT USING THE DKW INEQUALITY

In this section, we propose a systematic approach for determining the parameters of Gaussian–Pareto overbounds based on the DKW inequality. This approach takes into the account the uncertainty of the empirical CDF obtained from finite data samples and allows for a quantifiable measure of confidence in overbounding the true distribution. The uncertainty of the empirical CDF is directly influenced by the amount of sample data.

2.1 | Impact of Data Size

The actual sensor error distribution is not always perfectly known in practice and must be inferred from finite data samples by constructing the empirical distribution based on the samples, which serves as the basis for developing overbounds. However, the accuracy of the empirical CDF is influenced by the sample size. Smaller sample sizes may lead to less accurate empirical estimates, potentially compromising the conservatism of the overbounds. Consider an example of the Student's t distribution, as shown in Figure 3. The Student's t distribution used in this example has a zero mean, degree of freedom $\nu = 5$, and standard deviation $\sigma = 0.05$. Four data sets were generated via Monte Carlo (MC) simulation by independently sampling from this Student's t distribution, with the number of samples in each data set equal to 10^3, 10^4, 10^5, and 10^6. Figure 3 displays the empirical CDFs derived from the sample data sets in comparison to the true CDF, with a focus on their left-hand tails. Several observations can be made.

- First, the accuracy of the empirical CDF in the tails improves as the sample size increases, e.g., the data set of size 10^3 characterizes the left-hand tail of the

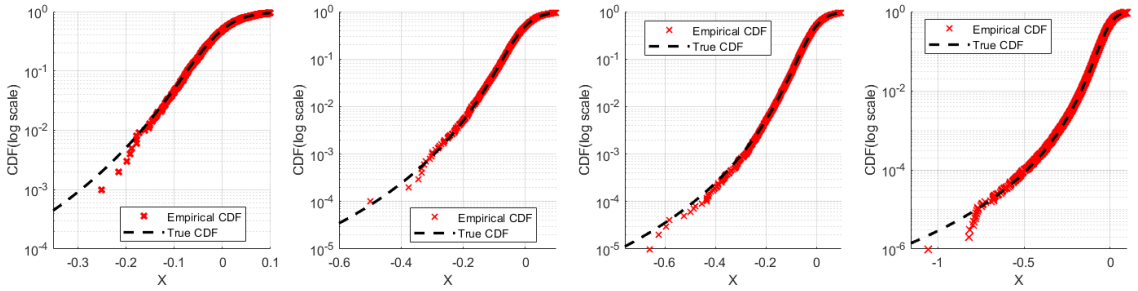

FIGURE 3 Comparison of the left-hand tails of the empirical CDFs (red) with the true CDFs (black) for different data sizes
The sizes of data samples are 10^3, 10^4, 10^5, and 10^6, from left to right.

CDF only up to a probability of 10^{-3}, whereas the data set of size 10^6 extends the left-hand tail characterization to the neighborhood of 10^{-6}.

- Second, modeling errors in the tails suggest that overbounds derived directly from empirical CDFs may fail to overbound the true distribution. As shown in Figure 3, the empirical CDF falls below the true CDF for data sets of sizes 10^3, 10^5, and 10^6. Consequently, an overbounding model constructed from such empirical CDFs could underestimate the true tail, potentially undermining system integrity. Thus, it is critical to account for the modeling errors of the empirical CDF due to limited sample sizes when designing overbounds for unknown error distributions.

2.2 | DKW Inequality

To address the potential impact of modeling errors in the empirical CDF, we must consider these errors carefully when developing overbounds for an unknown distribution. The example in Section 2.1 qualitatively illustrates how modeling errors decrease with increased data size and also warns of the possibility that the empirical CDF might underestimate the true distribution's tail, which could compromise the conservatism of the overbound. To systematically address this issue, a statistical tool known as the DKW inequality is employed to quantitatively characterize the relationship between modeling errors and sample size. The DKW inequality provides a confidence interval within which the true, unknown CDF is expected to lie, with a computed confidence level that depends on both the sample size and the width of the interval. By incorporating this CDF interval, the overbounding model can accommodate potential errors inherent in the sampled data, thereby enhancing the reliability of overbounding the true distribution. The mathematical form of the DKW inequality (Massart, 1990) is expressed as follows:

$$\mathbf{Pr}\left(\sup_{x\in\mathbb{R}}\left|\hat{F}_n(x)-F(x)\right|>\epsilon\right)\leq 2e^{-2n\epsilon^2} \quad \text{for every} \quad \epsilon>0 \tag{6}$$

where $F(x)$ denotes the CDF of the random variable X. $\hat{F}_n(x)$ is the empirically determined CDF, defined by $\hat{F}_n(x)=\frac{1}{n}\sum_{i=1}^{n}\left|\mathbb{1}_{(x_i\leq x)}\right|$, where $x_1, x_2, \cdots, x_n$ are real-valued samples independently and identically drawn from the distribution of the random variable X and n is the number of independent and identically distributed samples. The probability of the true CDF $F(x)$ exceeding the region formed

by shifting the empirical CDF $\hat{F}_n(x)$ up and down by a margin ϵ is bounded by the threshold $2e^{-2n\epsilon^2}$. This probability threshold $2e^{-2n\epsilon^2}$ is only dependent on the sample size n and margin ϵ.

The DKW inequality calculates the CDF interval within which the true underlying distribution may lie, with a specified level of confidence. The overbounding model can be developed by leveraging this CDF interval to accommodate the modeling errors inherent in empirical CDFs. We use a concrete example here to demonstrate how the DKW inequality can be incorporated into the overbound development. Similarly, the underlying error distribution is set to be the same Student's t distribution with zero mean, degree of freedom $\nu = 5$, and standard deviation $\sigma = 0.05$, as in Section 2.1. The PDF of the error distribution is symmetric around zero and has heavy tails. We will construct the Gaussian–Pareto and Gaussian models to overbound the underlying error distribution.

2.3 | Gaussian–Pareto Overbound

Larson et al. (2019a) provided an estimation procedure for Gaussian–Pareto overbounding. However, as noted in Section 1.2, an empirical approach is utilized in that work to adjust the GPD parameters to increase the conservatism, and a systematic assessment of how well the Gaussian–Pareto model reliably overbounds the true distribution remains unaddressed. By utilizing the DKW inequality in the Gaussian–Pareto approach, we can obtain a confidence interval that bounds the true CDF with a specified level of certainty. This approach enables us to construct the Gaussian–Pareto overbound based on this CDF interval, thereby ensuring that the overbound accounts for the modeling errors in the empirical CDF. Moreover, a quantifiable measure of confidence in overbounding the true distribution can be determined by the DKW-calculated probability.

We begin by collecting data from the underlying Student's t distribution. A total of 4×10^6 samples are drawn from this distribution. An empirical CDF can then be derived based on this sampled data set. Next, we partition the CDF into its core and tail regions by selecting thresholds for left-hand and right-hand tails. The partition is a trade-off between tail modeling accuracy and core conservatism. For example, consider the right-hand tail: if the threshold u_R is too large, the number of data points that exceed u_R will be small, resulting in a large estimation error for the GPD parameters. Meanwhile, a large tail threshold also indicates that the conservatism will increase in the Gaussian core. In contrast, if the threshold is decreased, the GPD fitting error will increase according to Equation (3). In this case, we select thresholds corresponding to the 0.001 and 0.999 quantiles for the left-hand and right-hand tails, respectively, such that approximately 4000 data points fall into each tail. The thresholds for the left-hand and right-hand tails are computed as $u_L = -0.2947$ and $u_R = 0.2947$, respectively.

After the entire distribution is partitioned into the core and tails, we next develop the core overbound using a Gaussian model. By using data samples from the core, we can calculate the CDF interval that bounds the core portion of the true CDF with a quantified level of confidence. Given a specified confidence ξ for overbounding the true CDF, the margin ϵ of the CDF interval can be computed using the probability provided by the DKW inequality, as follows:

$$\epsilon = \sqrt{\frac{1}{n}\log\sqrt{\frac{2}{1-\xi}}} \tag{7}$$

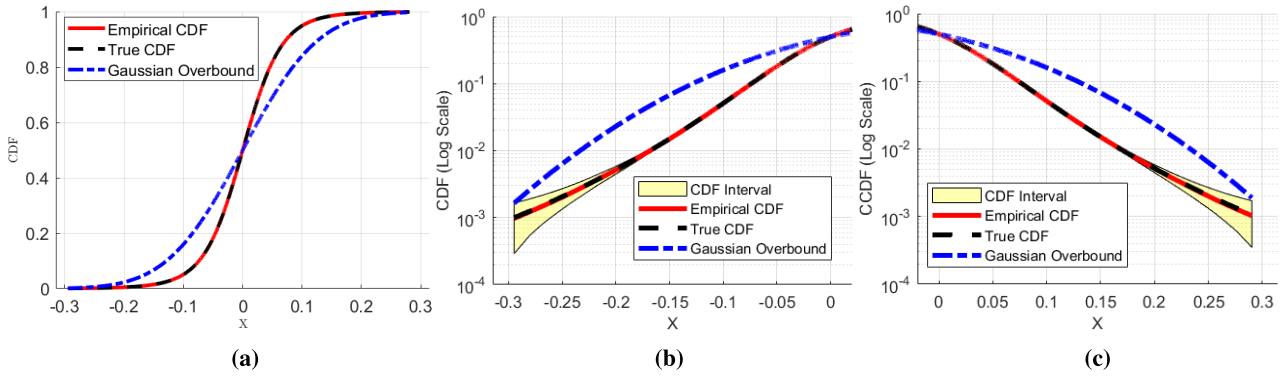

FIGURE 4 (a) CDF of the Gaussian overbound (blue dash-dotted) for the core of the distribution in comparison with the true CDF (black dashed) and the empirical CDF (red solid); (b) CDFs of the left end of the core of the distribution on a logarithmic scale; (c) complementary CDFs (CCDFs) of the right end of the core of the distribution on a logarithmic scale

In this example, if the level of confidence is set to 95% and the number of samples in the core is equal to 4×10^6, the margin ϵ of the CDF interval can be calculated as 6.80×10^{-4}. Thereby, the confidence CDF interval can be determined by shifting the empirical CDF up and down by the margin 6.80×10^{-4}, giving us 95% confidence that the core of the true CDF falls within the CDF interval. The Gaussian overbound can then be determined to overbound the CDF interval. Figure 4(a) shows the Gaussian overbounding model for the core of the underlying distribution in this example. Figures 4(b) and (c) zoom into the left and right ends of the core distribution. The confidence CDF interval calculated by the DKW inequality is denoted by the yellow region that encompasses both the true CDF (black dashed) and the empirical CDF (red solid). To ensure overbounding of the true CDF, the Gaussian overbounding model (blue dash-dotted) is developed to tightly overbound the CDF interval. The mean of the Gaussian overbound is zero, and the standard deviation is determined to be 0.1004. Thus, we have 95% confidence that this Gaussian distribution can overbound the core of the true CDF, according to the DKW inequality.

After establishing the Gaussian overbound for the core of the distribution, we proceed to construct the generalized Pareto overbounds for the tails using the EVT method. The EVT method operates on the tail portion of a distribution in the CEDF domain. Thus, we must convert the tails from the CDF domain to the CEDF domain. Taking the right-hand tail as an example, the CEDF of the right-hand tail can be computed using Equation (2). Figure 5(a) shows both the true CEDF of the underlying distribution (black dashed) and the empirical CEDF (red solid) for the right-hand tail. In addition, the complementary CEDF plot is provided on a logarithmic scale in Figure 5(b) for better visualization of the tail behavior. The number of samples in the right-hand tail is 3854. If we want to maintain a 95% confidence level in overbounding the true CEDF for the right-hand tail, the margin of the confidence interval in the CEDF domain is calculated as 0.0219 based on Equation (7). Thereby, the confidence interval can be determined as the yellow region in Figure 5.

Next, the EVT method is applied to develop the generalized Pareto overbound for the right-hand tail. The GPD parameters γ and β are estimated using the MLE method. In this example, we use the MATLAB function `gpfit` to obtain the maximum likelihood estimates of these two parameters. The estimated GPD parameters for the right-hand tail are $\hat{\gamma}=0.1618$ and $\hat{\beta}=0.0674$. In Figures 5(a) and (b), the estimated GPD is shown by a dark green dotted line. Figure 5(a) shows that

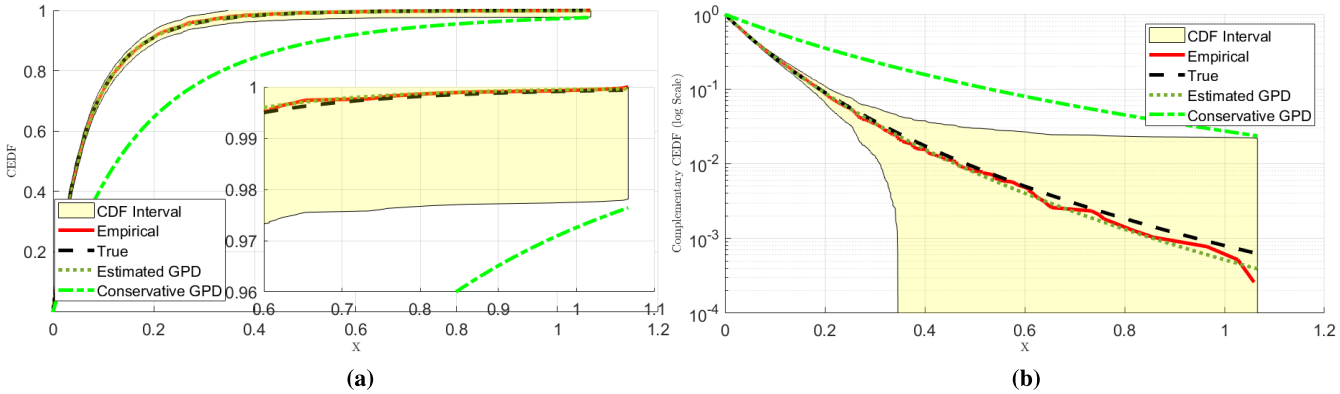

FIGURE 5 (a) Comparison of CEDF curves for the right-hand tail of the distribution; (b) complementary CEDF of the curves from Figure 5(a) displayed on a logarithmic scale
In (a), the confidence CDF interval (yellow region) with margin $\epsilon = 0.0219$ and confidence level 95% is determined by using the DKW inequality. The true CEDF (black dashed) and empirical CEDF (red solid) are encompassed by this confidence interval. The estimated GPD (dark green dotted) is an approximation to the empirical CEDF based on EVT. The conservative GPD model (light green dash-dotted) overbounds the confidence region, thus the true CEDF, with the specified confidence level.

the true CEDF, empirical CEDF, and estimated GPD are very close to each other. Figure 5(b), with a logarithmic scale, provides a clearer view of the discrepancies between these curves. To overbound the true unknown CEDF with the specified level of confidence, the conservative GPD should overbound the yellow confidence interval determined by the DKW inequality. Thus, we must adjust the GPD parameters to achieve the conservative GPD overbound. By inspecting the conservatism of the GPD curve with respect to the yellow region, we can determine the conservative GPD overbound (light green dash-dotted) with the adjusted parameters $\hat{\gamma}' = 0.2618$ and $\hat{\beta}' = 0.1674$. Similarly, the same approach can be applied to develop the conservative GPD overbound for the left-hand tail of the underlying error distribution. Figures 6(a) and (b) show the conservative GPD (light green dash-dotted) that overbounds the confidence interval (yellow region) for the CEDF of the left-hand tail. The parameters related to the Gaussian overbound for the core and the generalized Pareto overbounds for the tails are summarized in Table 1.

The developed generalized Pareto overbounds for the tails, along with their confidence intervals, are expressed in the CEDF domain. To construct the complete piece-wise Gaussian–Pareto overbound, we must convert these tail overbounds back into the CDF domain. Equation (5) can be used to convert CEDFs back to CDFs. Once transformed, the tail overbounds can be combined with the Gaussian overbound for the core, forming a unified Gaussian–Pareto overbound across the entire distribution. Additionally, to satisfy the requirement of zero mean, symmetry, and unimodality for the overbounds (DeCleene, 2000), the generalized Pareto overbounds for the left-hand and right-hand tail must be unified to maintain the symmetry of the Gaussian–Pareto PDF. Thus, we select the more conservative generalized Pareto overbound and use it to overbound both tails. For instance, by comparing the overbounding parameters in Table 1, it can be seen that $\hat{\gamma}'_{\mathrm{L}} > \hat{\gamma}'_{\mathrm{R}}$ and $\hat{\beta}'_{\mathrm{L}} > \hat{\beta}'_{\mathrm{R}}$, which indicates that the generalized Pareto of the left-hand tail is more conservative than that of the right-hand tail. We assign the left-tail overbounding parameters to the right tail to preserve the symmetry of the PDF. Consequently, the Gaussian–Pareto overbounding model is established, and its parameters are listed in Table 2. We plot the CDF of the Gaussian–Pareto overbound (blue dash-dotted) alongside the empirical CDF (blue solid) and the true CDF (black dashed) of the

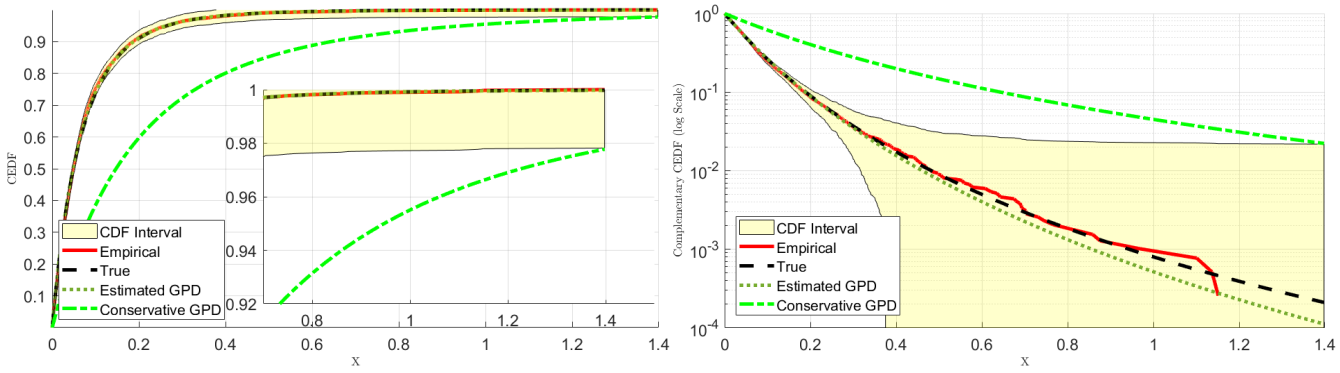

FIGURE 6 (a) Comparison of CEDF curves for the left-hand tail of the distribution; (b) complementary CEDF of the curves from Figure 6(a) displayed on a logarithmic scale
In (a), the confidence CDF interval (yellow region) with margin $\epsilon = 0.0218$ and confidence level 95% is determined by using the DKW inequality. The true CEDF (black dashed) and empirical CEDF (red solid) are encompassed by this confidence interval. The estimated GPD (dark green dotted) is an approximation to the empirical CEDF based on EVT. The conservative GPD model (light green dash-dotted) overbounds the confidence region, thus the true CEDF, with the specified confidence level.

TABLE 1
Summary of Overbounding Parameters for the Core and Tail Portions of the Underlying Student's t Distribution with Zero Mean, Degree of Freedom $\nu = 5$, and Standard Deviation $\sigma = 0.05$

	Core	Left-hand Tail	Right-hand Tail
Sample size n	3.9922×10^6	3879	3854
Confidence level ξ	95%	95%	95%
Interval margin ϵ	6.8000×10^{-4}	0.0218	0.0219
Overbounding model	Gaussian overbound	generalized Pareto overbound	generalized Pareto overbound
Overounding parameters	$\mu = 0, \sigma = 0.1004$	$\hat{\gamma}'_{\mathrm{L}} = 0.3154, \hat{\beta}'_{\mathrm{L}} = 0.1900$	$\hat{\gamma}'_{\mathrm{R}} = 0.2618, \hat{\beta}'_{\mathrm{R}} = 0.1674$

TABLE 2
Parameters of the Gaussian–Pareto Distribution to Overbound a Student's t Distribution with Zero Mean, Degree of Freedom $\nu = 5$, and Standard Deviation $\sigma = 0.05$

Left-hand Tail Threshold u_{L}	–0.2947	**Right-hand Tail Threshold u_{R}**	0.2947
Left-hand Tail GPD $\hat{\gamma}'_{\mathrm{L}}$	0.3154	**Right-hand Tail GPD $\hat{\gamma}'_{\mathrm{R}}$**	0.3154
Left-hand Tail GPD $\hat{\beta}'_{\mathrm{L}}$	0.1900	**Right-hand Tail GPD $\hat{\beta}'_{\mathrm{R}}$**	0.1900
Core Mean μ	0	**Core Standard Deviation σ**	0.1004

Student's t distribution in Figure 7. Figures 7(b) and (c) provide zoomed-in views of the tail-overbounding on a logarithmic scale. The CDF intervals (yellow region) for both the core and tail portions are determined by the DKW inequality with a 95% confidence level that encompasses the true CDF, which is usually unknown in practice. As shown, the Gaussian–Pareto distribution can effectively overbound the CDF interval, thus ensuring the overbounding of the true underlying distribution with the specified 95% confidence level. Additionally, a Gaussian overbound (cyan dotted) is also included in Figure 7 for comparison with the Gaussian–Pareto overbound. Because of the heavy tails of the Student's t distribution, the variance of the Gaussian overbound must be inflated to a great extent to overbound the heavy

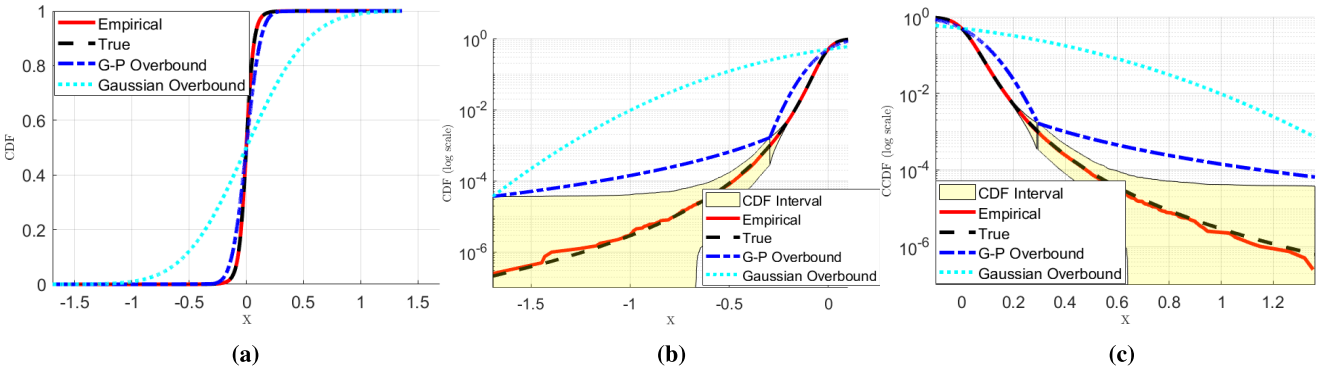

FIGURE 7 (a) Comparison of the CDFs of the Gaussian–Pareto (G-P) overbound (blue dash-dotted) and Gaussian overbound (cyan dotted); (b) zoomed-in view of the left-hand tail on a logarithmic scale; (c) CCDF of the right-hand tail on a logarithmic scale
In (a), the Gaussian–Pareto model provides a tighter overbound compared with the Gaussian distribution. In (b), the CDF interval (yellow region) encompasses the true CDF (black dashed) and the empirical CDF (red solid) with the specified confidence level 95%. Both the G-P overbound and Gaussian overbound can bound the CDF interval. In (c), the right tail is also bounded by the G-P overbound and Gaussian overbound.

tails. In this example, the standard deviation of the Gaussian overbound is calculated as 0.4269 to overbound the same CDF interval as illustrated in Figures 7(b) and (c). The Gaussian–Pareto distribution is a much tighter overbound than the Gaussian overbound, which, in contrast, exhibits excessive conservatism. Thereby, Gaussian–Pareto overbounds have the potential to increase the availability of PNT systems when applied to safety-critical applications.

3 | A CONSERVATIVE GMM APPROACH

3.1 | Motivation

EVT and the DKW inequality provide the basis for developing Gaussian–Pareto overbounds to conservatively model sensor uncertainties with heavy-tailed characteristics for safety-critical navigation systems. Despite their potential for increasing the availability of PNT systems, Gaussian–Pareto distributions do not have clear convolution properties similar to those of Gaussian distributions, which restricts their direct application within PNT filtering frameworks. To overcome this limitation, we propose a novel approach that conservatively fits the Gaussian–Pareto distribution using a GMM. This approach preserves the tight overbounding characteristics of the Gaussian–Pareto model while taking advantage of the convolution properties of Gaussian distributions, facilitating density propagation within recursive filtering processes.

The topic of GMMs has been extensively studied in the existing literature, particularly in the PNT and robotics domains, where GMMs are often used to model non-Gaussian noise or distributions. Lee (2004) and Blanch et al. (2008) employed a bimodal Gaussian mixture to model heavy-tailed error distributions. Y. Yun et al. (2008) assumed that the pseudorange error follows a Gaussian-core-Laplacian-tail (GCLT) distribution and used a GMM to approximate this distribution. However, the GCLT model does not inherently ensure that it overbounds the true underlying distribution, and Y. Yun et al. (2008) did not discuss the parameter determination process for the GMM. The GMM estimation using the expectation-maximization (EM) approach was discussed by Reynolds (2009). The EM algorithm relies directly

on data samples drawn from the underlying error distribution. However, the resulting GMM is not guaranteed to overbound the true error distribution. H. Yun et al. (2011) formed an optimization-based approach for estimating GMM parameters, but this method assumes perfect knowledge of the non-Gaussian error distribution. Furthermore, the estimated GMM in this case is still not guaranteed to act as an overbound of the actual error distribution.

In the context of integrity for safety-critical PNT systems, existing GMM estimation approaches are inadequate for the following reasons. First, these methods focus on modeling GMMs to represent the underlying error distribution. However, there is no guarantee that the resulting GMM overbounds the underlying distribution. Second, in most practical scenarios, the true error distribution is unknown, and GMMs are constructed based on sampled data. As discussed in Section 2.1, a limited sample size introduces modeling errors into the GMM estimation process, potentially compromising the accuracy and conservatism of the GMM. These limitations highlight the need for our proposed conservative GMM estimation approach, which is designed to directly address these challenges.

In contrast, our proposed approach avoids directly modeling the unknown underlying error distribution. Instead, it fits a GMM to the Gaussian–Pareto overbound, which is developed to overbound the unknown underlying distribution. This strategy offers two key advantages. First, the modeling errors introduced by the limited sample size are already accounted for in the Gaussian–Pareto overbound through the use of the DKW inequality. As a result, the GMM estimated to approximate the Gaussian–Pareto overbound is expected to overbound the underlying error distribution while accounting for the modeling errors of the limited sampled data. Second, despite imperfect knowledge of the underlying error distribution, the Gaussian–Pareto overbound is fully known to us. Thus, our proposed GMM estimation approach does not rely on sampled data. Instead, this approach directly fits the PDF curve of the Gaussian–Pareto overbound, thereby eliminating the sampling-induced uncertainty.

3.2 | Methodology

Figure 8 illustrates the intuition behind our GMM estimation approach. In this figure, a series of Gaussian PDFs are distributed along the x axis. When the standard deviations of these Gaussians are relatively small, their PDF shapes resemble spikes. As the standard deviation approaches zero, the PDF height increases indefinitely, approaching an impulse function. These Gaussian PDFs are evaluated as approximately zero everywhere except within a small neighborhood around their means. Consequently, a GMM, composed of multiple such Gaussian components, can flexibly approximate complex distributions by strategically adjusting the spread and weights of individual Gaussian distributions.

For a random variable X, the PDF of a GMM can be represented as a weighted sum of individual Gaussian components:

$$f_{\mathrm{GMM}}(x)=\sum_{k=1}^{n}\lambda_k\mathcal{N}\left(x\,|\,\mu_k,\sigma_k^2\right)=\sum_{k=1}^{n}\lambda_k\frac{1}{\sigma_k\sqrt{2\pi}}\exp\left\{-\frac{1}{2}\left(\frac{x-\mu_k}{\sigma_k}\right)^2\right\} \tag{8}$$

where n is the number of Gaussian components in the mixture, λ_k is the weight associated with the k-th Gaussian component, which must satisfy $\sum_{k=1}^{n}\lambda_k=1$, and

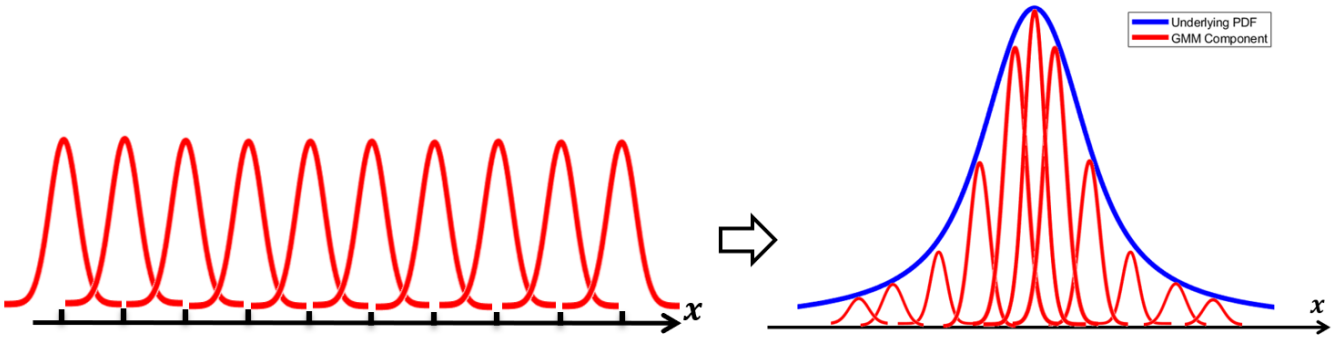

FIGURE 8 The target distribution (blue) can be approximated by a series of Gaussian components (red), which are evenly spaced along the support of x.

$\mathcal{N}(x \mid \mu_k, \sigma_k^2)$ denotes the Gaussian PDF with mean μ_k and variance σ_k^2. The parameters $\{\lambda_k, \mu_k, \sigma_k\}_{k=1}^n$ should be determined to obtain the GMM that best fits the target distribution.

As discussed in Section 3.1, our objective is to fit a GMM to the Gaussian–Pareto distribution, which is developed to overbound the underlying error distribution. This task falls into the category of curve-fitting problems. Given that the Gaussian–Pareto model is fully known, data points for the fitting process can be precisely generated from the Gaussian–Pareto PDF, ensuring an accurate basis for the GMM approximation. We select m data points $\{x_j, f_{\text{G-P}}(x_j)\}_{j=1}^m$ from the Gaussian–Pareto PDF curve. To each data point $\{x_j, f_{\text{G-P}}(x_j)\}$, we assign a weighting coefficient ω_j, which reflects the importance of that particular point. For instance, higher weights can be assigned to data points in the tail regions to prioritize accurate fitting of the tails over the core region, if desired. It is important to distinguish between the GMM weights λ_k and the weighting coefficients ω_j used for the curve-fitting data points. Next, this curve-fitting problem can be formulated as follows:

$$\min_{\{\lambda_k, \mu_k, \sigma_k\}_{k=1}^n} \quad \sum_{j=1}^{m} \omega_j \left\| f_{\text{G-P}}(x_j) - \sum_{k=1}^{n} \lambda_k \mathcal{N}(x_j \mid \mu_k, \sigma_k^2) \right\|^2 \quad \text{s.t.} \quad \sum_{k=1}^{n} \lambda_k = 1 \tag{9}$$

Equation (9) represents a constrained nonlinear least-square problem with optimization variables $\{\lambda_k, \mu_k, \sigma_k\}_{k=1}^n$. Solving this optimization yields the GMM that best fits the Gaussian–Pareto overbound. However, one critical requirement of the GMM modeling in the context of safety-critical PNT is that the conservatism of the Gaussian–Pareto overbound must be preserved in the estimated GMM. This requirement ensures that the underlying error distribution is reliably overbounded by the GMM. However, the current problem formulation in Equation (9) does not inherently guarantee this conservatism preservation. For instance, if the tail of the target PDF is on the order of 10^{-4} and the tail of the GMM PDF is on the order of 10^{-6}, the discrepancy in the tails contributes minimally to the objective function compared with the PDF discrepancies in the core. This imbalance causes the optimization process to focus more on fitting the core, making it insufficiently sensitive to the accuracy of tail-fitting, where conservatism is most critical. One possible way to increase the tail-fitting accuracy is by increasing the weight coefficients ω_j assigned to the data points in the tail regions. However, this approach is highly heuristic and does not systematically guarantee that the resulting GMM still

overbounds the underlying error distribution. To overcome this limitation, we propose to directly impose constraints on tail-fitting within the optimization formulation. These constraints ensure that the GMM preserves the overbounding property of the Gaussian–Pareto model.

For instance, Figure 7 shows the Gaussian–Pareto distribution developed to overbound the underlying error distribution. We denote the right endpoint and left endpoint of the sampled data by $x_{\mathrm{R,end}}$ and $x_{\mathrm{L,end}}$, respectively. In the example presented in Figure 7, $x_{\mathrm{L,end}} = -1.6928$ and $x_{\mathrm{R,end}} = 1.3608$. As the Gaussian–Pareto distribution overbounds the true underlying distribution, the CDFs of the Gaussian–Pareto $F_{\mathbf{G\text{-}P}}(x)$ and true distribution $F_{\mathbf{true}}(x)$ satisfy the following the relationships at the left-hand and right-hand tails:

$$F_{\mathbf{G\text{-}P}}\left(x_{\mathrm{L,end}}\right) \geq F_{\mathbf{true}}\left(x_{\mathrm{L,end}}\right), \quad F_{\mathbf{G\text{-}P}}\left(x_{\mathrm{R,end}}\right) \leq F_{\mathbf{true}}\left(x_{\mathrm{R,end}}\right) \tag{10}$$

To preserve the conservatism such that the estimated GMM still overbounds the true underlying distribution, we can impose the following constraints:

$$F_{\mathbf{GMM}}\left(x_{\mathrm{L,end}}\right) \geq F_{\mathbf{G\text{-}P}}\left(x_{\mathrm{L,end}}\right), \quad F_{\mathbf{GMM}}\left(x_{\mathrm{R,end}}\right) \leq F_{\mathbf{G\text{-}P}}\left(x_{\mathrm{R,end}}\right) \tag{11}$$

such that:

$$\begin{aligned} &F_{\mathbf{GMM}}\left(x_{\mathrm{L,end}}\right) \geq F_{\mathbf{G\text{-}P}}\left(x_{\mathrm{L,end}}\right) \geq F_{\mathbf{true}}\left(x_{\mathrm{L,end}}\right), \\ &F_{\mathbf{GMM}}\left(x_{\mathrm{R,end}}\right) \leq F_{\mathbf{G\text{-}P}}\left(x_{\mathrm{R,end}}\right) \leq F_{\mathbf{true}}\left(x_{\mathrm{R,end}}\right) \end{aligned} \tag{12}$$

Equation (12) indicates that the GMM can overbound the true underlying distribution at both the left-hand and right-hand tails if the condition in Equation (11) is met. To enforce this tail-overbounding requirement, we incorporate Equation (11) as additional constraints into the nonlinear least-square problem in Equation (9) to overcome the challenge of the tail-fitting imbalance and preserve the conservative tail behavior in the GMM estimation, thus ensuring a robust and reliable overbound for the true underlying distribution. The modified GMM estimation problem formulation can be expressed as follows:

$$\begin{aligned} \min_{\{\lambda_k,\mu_k,\sigma_k\}_{k=1}^{n}} \quad & \sum_{j=1}^{m} \omega_j \left\| f_{\mathrm{G\text{-}P}}(x_j) - \sum_{k=1}^{n} \lambda_k \mathcal{N}(x_j \mid \mu_k, \sigma_k^2) \right\|^2 \\ \text{s.t.} \quad & \sum_{k=1}^{n} \lambda_k = 1, \\ & \sum_{k=1}^{n} \lambda_k F_{\mathrm{Gau}}(x \mid \mu_k, \sigma_k^2)\big|_{x=x_{\mathrm{L,end}}} \geq F_{\mathbf{G\text{-}P}}(x_{\mathrm{L,end}}), \\ & \sum_{k=1}^{n} \lambda_k F_{\mathrm{Gau}}(x \mid \mu_k, \sigma_k^2)\big|_{x=x_{\mathrm{R,end}}} \leq F_{\mathbf{G\text{-}P}}(x_{\mathrm{R,end}}) \end{aligned} \tag{13}$$

where $F_{\mathrm{Gau}}\left(x \mid \mu_k, \sigma_k^2\right)$ denotes the CDF of the Gaussian distribution with mean μ_k and variance σ_k^2. The terms $F_{\mathbf{G\text{-}P}}\left(x_{\mathrm{L,end}}\right)$ and $F_{\mathbf{G\text{-}P}}\left(x_{\mathrm{R,end}}\right)$ are both known values, as the Gaussian–Pareto overbound is fully defined, and the endpoints $x_{\mathrm{L,end}}, x_{\mathrm{R,end}}$ can be determined from the sampled data. Solving the constrained optimization problem in Equation (13) yields the GMM that best fits the Gaussian–Pareto overbound while preserving the conservative tail-overbounding behavior.

3.3 | Solving the GMM Estimation Problem

The constrained nonlinear optimization problem in Equation (13) is non-convex, making it challenging to guarantee a global solution. While a global minimum is not strictly required for our application—as long as conservative overbounding is preserved without undue conservatism—the non-convexity complicates obtaining a tractable and reliable solution. Nonlinear programming solvers, such as MATLAB's `fmincon` function, can be utilized to solve for a local minimum. In this paper, we propose an alternative solution that prioritizes computational tractability and efficiency by introducing a simplified formulation that yields a closed-form solution for the conservative GMM estimation. While this approach does not guarantee the least-conservative approximation, it provides a provable overbound that can be efficiently computed and integrated into recursive filtering frameworks. To better illustrate this approach, we use the same example discussed in Section 2, where the underlying error distribution follows a Student's t distribution and a Gaussian–Pareto model is developed to overbound it, as shown in Figure 7.

First, we identify the right endpoint $x_{\text{R,end}}$ and the left endpoint $x_{\text{L,end}}$ from the sampled data. In this example, $x_{\text{R,end}} = 1.3608$ and $x_{\text{L,end}} = -1.6928$. Next, we define the variable x_{end} as the larger of the two absolute values of $x_{\text{L,end}}$ and $x_{\text{R,end}}$, which gives us $x_{\text{end}} = 1.6928$. Thus, we obtain the range $[-x_{\text{end}}, x_{\text{end}}]$ over which the Gaussian–Pareto overbound can overbound the underlying Student's t distribution with 95% confidence. Consequently, our goal is for the estimated GMM, which best fits the Gaussian–Pareto overbound, to also overbound the underlying Student's t distribution over the same range $[-x_{\text{end}}, x_{\text{end}}]$.

Next, we select m data points, denoted $\{x_j, f_{\text{G-P}}(x_j)\}_{j=1}^{m}$, from the PDF of the Gaussian–Pareto overbound. For this example, we set $m = 5000$. These selected data points should ideally span the Gaussian–Pareto distribution comprehensively. An important guideline for choosing the range of the selected data points is that it should at least encompass the specified overbounding range $[-x_{\text{end}}, x_{\text{end}}]$ to ensure accurate fitting, particularly in the tails of the Gaussian–Pareto overbound. Thereby, we choose the range [–2, 2] for selecting data points in this example. Specifically, $\{x_j\}_{j=1}^{5000}$ are evenly distributed across the range [–2, 2]. The corresponding $\{f_{\text{G-P}}(x_j)\}_{j=1}^{5000}$ values can be computed by evaluating the Gaussian–Pareto PDF at each x_j. Hence, the data set $\{x_j, f_{\text{G-P}}(x_j)\}_{j=1}^{5000}$ for curve-fitting is established.

Then, we introduce our modifications to the original problem in Equation (13) to simplify the non-convex optimization. To reduce the complexity of the original optimization problem, we specify that the means of the Gaussian mixture components are evenly spaced along the x axis and that all components share the same variance, i.e., $\sigma_k^2 = \sigma^2$ for all k. This adjustment fixes the mean of each individual Gaussian component, reducing the number of parameters to optimize. Additionally, we must determine the appropriate range for the means of the Gaussian components. Similar to the range determination for the curve-fitting data set, the range for the Gaussian component means should ideally cover the Gaussian–Pareto distribution comprehensively as well. A similar guideline applies: the range for the Gaussian component means should at least encompass the specified overbounding range $[-x_{\text{end}}, x_{\text{end}}]$ to ensure accurate tail-fitting of the Gaussian–Pareto overbound. For this example, we set the number of Gaussian components to $n = 100$ and align the range for the Gaussian component means with the range of the curve-fitting data points [–2, 2]. Thus, $\{\mu_k\}_{k=1}^{100}$ are evenly distributed across the range [–2, 2].

As noted in Section 2.3, we applied the symmetry requirement to the Gaussian–Pareto distribution. For consistency, this symmetry constraint should also be imposed on the GMM. The means of the Gaussian components are evenly

distributed along the x axis, and all of the Gaussian components share a common variance. Thus, to achieve symmetry in the GMM, we must assign symmetric weights across the x axis. For this example, the means of the Gaussian components are evenly spaced along the range [–2, 2]. For each Gaussian component with mean μ_k and weight λ_k, there is a corresponding component with mean $\mu_{n-k+1} = -\mu_k$ and an identical weight $\lambda_{n-k+1} = \lambda_k$. Therefore, the design variables of weight $\{\lambda_k\}_{k=1}^{n}$ can be reduced to $\{\lambda_k\}_{k=1}^{n/2}$ (if n is an even number) or $\{\lambda_k\}_{k=1}^{(n+1)/2}$ (if n is an odd number). The PDF of the symmetric GMM, using the reduced number of variables, can be rewritten as follows:

$$f_{\text{GMM}}(x) = \sum_{k=1}^{(n+1)/2} \lambda_k \mathcal{N}\left(x \,|\, \mu_k, \sigma^2\right) + \sum_{k=1}^{(n-1)/2} \lambda_k \mathcal{N}\left(x \,|\, -\mu_k, \sigma^2\right), \quad \text{if n is an odd number} \tag{14a}$$

$$f_{\text{GMM}}(x) = \sum_{k=1}^{n/2} \lambda_k \mathcal{N}\left(x \,|\, \mu_k, \sigma^2\right) + \sum_{k=1}^{n/2} \lambda_k \mathcal{N}\left(x \,|\, -\mu_k, \sigma^2\right), \quad \text{if n is an even number} \tag{14b}$$

Accordingly, the original GMM estimation formulation in Equation (13) can be rewritten as follows:

$$\begin{aligned} \min_{\{\lambda_k\}_{k=1}^{n/2}, \sigma} \quad & \sum_{j=1}^{m} \omega_j \left\| f_{\text{G-P}}(x_j) - \sum_{k=1}^{n/2} \lambda_k \mathcal{N}(x_j \,|\, \mu_k, \sigma^2) - \sum_{k=1}^{n/2} \lambda_k \mathcal{N}(x_j \,|\, -\mu_k, \sigma^2) \right\|^2 \\ \text{s.t.} \quad & 2\sum_{k=1}^{n/2} \lambda_k = 1, \\ & \sum_{k=1}^{n/2} \lambda_k F_{\text{Gau}}(x \,|\, \mu_k, \sigma^2)\big|_{x=-x_{\text{end}}} + \sum_{k=1}^{n/2} \lambda_k F_{\text{Gau}}(x \,|\, -\mu_k, \sigma^2)\big|_{x=-x_{\text{end}}} \geq F_{\text{G-P}}(-x_{\text{end}}) \end{aligned} \tag{15}$$

Equation (15) represents the formulation for the symmetric GMM estimation when the number of Gaussian components n is even. The optimization variables are reduced to the symmetric weights $\{\lambda_k\}_{k=1}^{n/2}$ and the shared standard deviation σ. Additionally, in contrast to Equation (13), the two tail-overbounding constraints are reduced to a single constraint because of the symmetric structure of the GMM and the Gaussian–Pareto overbound. However, the optimization in Equation (15) remains non-convex owing to the optimization variable σ. Thus, to further simplify the optimization, we set the common variance σ^2 to a predefined value. We found a good rule of thumb for empirically determining σ by dividing half of the range length of the Gaussian component means by the number of Gaussian components. For this example, the Gaussian component means are spread over $[-2, 2]$ and $n = 100$. Thus, the common standard deviation can be calculated as $\sigma = 2/100 = 0.02$. Note that the empirically determined standard deviation serves as a rough initial estimate, which may be subject to further tuning to improve the fitting accuracy. Here, we simply use $\sigma = 0.02$ for the shared standard deviation.

After the standard deviation σ is determined, Equation (15) is simplified into a standard least-square problem with constraints, as shown in Equation (16). The only optimization variables are the Gaussian component weights, and the optimization problem now becomes convex. We derive a closed-form solution to the optimization in Equation (16) in Appendix A. The estimated conservative GMM is illustrated in Figure 9. It can be seen that the estimated GMM (magenta dash-dotted) closely follows the Gaussian–Pareto overbound (blue dash-dotted). Figures 9(b) and (c) highlight the tail-overbounding performance on a logarithmic scale. We observe

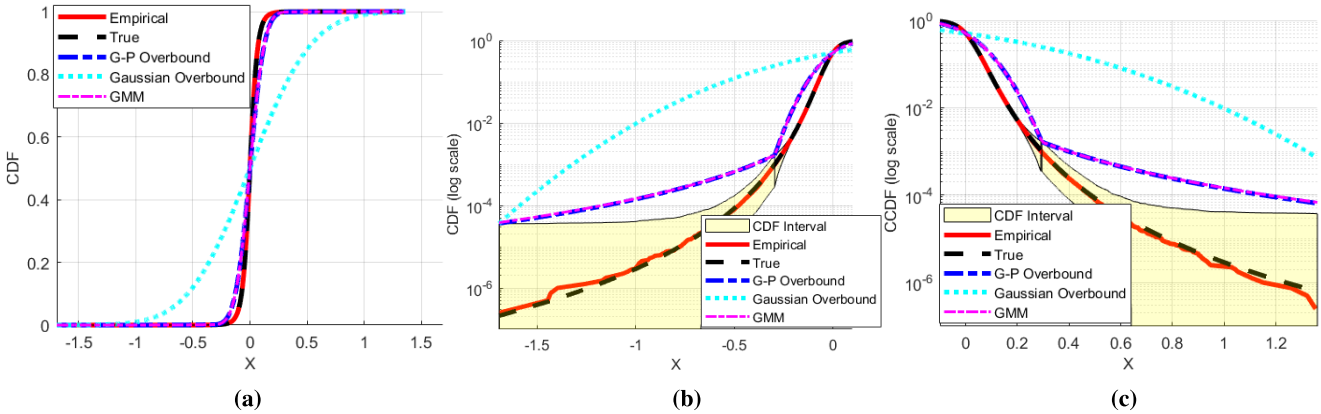

FIGURE 9 (a) Comparison of the estimated conservative GMM (magenta dash-dotted) and Gaussian–Pareto (G-P) overbound (blue dash-dotted); (b) zoomed-in view of the left-hand tail on a logarithmic scale; (c) CCDF of the right-hand tail on a logarithmic scale
Panel (a) shows that the GMM can closely follow the Gaussian–Pareto overbound. In (b), the CDF interval (yellow region) encompasses the true CDF (black dashed) and the empirical CDF (red solid) with the specified confidence level of 95%. The estimated GMM is almost overlapping with the G-P overbound. Both the GMM and G-P distribution can bound the CDF interval. In (c), the right-hand tail is also bounded by the GMM and G-P overbound.

ALGORITHM 2
Conservative GMM Estimation

INPUT: Gaussian–Pareto Overbound $F_{\text{G-P}}(x)$
OUTPUT: Conservative GMM $F_{\text{GMM}}(x)$

1: Determine the right endpoint $x_{\text{R,end}}$ and left endpoint $x_{\text{L,end}}$ from the sampled data
2: Define variable $x_{\text{end}} \leftarrow \max(|x_{\text{R,end}}|, |x_{\text{L,end}}|)$
3: Select the number of data points m for curve-fitting and the number of Gaussian mixture components n
4: Determine the range of the curve-fitting data points and the range of the Gaussian component means to encompass $[-x_{\text{end}}, x_{\text{end}}]$
5: Obtain the curve-fitting data set $\{x_j, f_{\text{G-P}}(x_j)\}_{j=0}^{m}$ that is evenly spread along the x axis
6: Specify the Gaussian component means $\{\mu_k\}_{k=0}^{n}$ to be evenly spaced along the x axis
7: Calculate the shared standard deviation σ
8: Solve Equation (16) for the GMM component weights $\{\lambda_k\}_{k=0}^{n}$
9: Obtain the conservative GMM using $\{\lambda_k\}_{k=0}^{n}$, $\{\mu_k\}_{k=0}^{n}$ and σ

that the estimated GMM almost overlaps with the Gaussian–Pareto overbound. Notably, both the estimated GMM and Gaussian–Pareto overbound can overbound the CDF interval (yellow region), which encompasses the true underlying CDF with 95% confidence, according to the DKW inequality. This proposed approach to solving the GMM estimation problem is summarized in Algorithm 2:

$$\begin{aligned}
\min_{\{\lambda_k\}_{k=1}^{\text{n}/2}} \quad & \sum_{j=1}^{m} \omega_j \left\| f_{\text{G-P}}(x_j) - \sum_{k=1}^{\text{n}/2} \lambda_k \mathcal{N}(x_j \,|\, \mu_k, \sigma^2) - \sum_{k=1}^{\text{n}/2} \lambda_k \mathcal{N}(x_j \,|\, -\mu_k, \sigma^2) \right\|^2 \\
\text{s.t.} \quad & 2\sum_{k=1}^{\text{n}/2} \lambda_k = 1, \\
& \sum_{k=1}^{\text{n}/2} \lambda_k F_{\text{Gau}}(x \,|\, \mu_k, \sigma^2)\big|_{x=-x_{\text{end}}} + \sum_{k=1}^{\text{n}/2} \lambda_k F_{\text{Gau}}(x \,|\, -\mu_k, \sigma^2)\big|_{x=-x_{\text{end}}} \geq F_{\textbf{G-P}}(-x_{\text{end}})
\end{aligned} \tag{16}$$

4 | RECURSIVE BAYESIAN OVERBOUNDING FILTER

The proposed conservative GMM estimation fits a GMM to the Gaussian–Pareto overbound. On one hand, the GMM retains the convolution properties of the Gaussian distribution, which effectively addresses the challenge of propagating Gaussian–Pareto distributions in PNT filters. On the other hand, the GMM preserves the overbounding characteristics of the Gaussian–Pareto distribution, which has the potential to increase the availability of safety-critical PNT systems. As illustrated by the input–output overbounding relationship in Figure 2, when the sensor error distribution is overbounded by the GMM, the next step is to design a PNT filter that uses the GMM overbound as input and provides a reliable overbound on the system output errors.

Consider the following linear discrete-time stochastic system with additive noise:

$$\begin{aligned} \mathbf{x}_{k+1} &= \mathbf{A}_k \mathbf{x}_k + \mathbf{w}_k, \quad \mathbf{w}_k \sim \mathcal{N}(\mathbf{0}, \mathbf{Q}_k) \\ \mathbf{y}_k &= \mathbf{H}_k \mathbf{x}_k + \mathbf{v}_k \end{aligned} \tag{17}$$

where $\mathbf{x}_k \in \mathbb{R}^{n\times 1}$ denotes the state vector of the system. $\mathbf{A}_k \in \mathbb{R}^{n\times n}$ represents the state transition matrix. The process noise $\mathbf{w}_k \in \mathbb{R}^{n\times 1}$ is assumed to be a Gaussian random variable with zero mean and covariance matrix $\mathbf{Q}_k \in \mathbb{R}^{n\times n}$. $\mathbf{y}_k \in \mathbb{R}^{m\times 1}$ denotes the measurement at time step k. $\mathbf{H}_k \in \mathbb{R}^{m\times n}$ is the measurement matrix, and the measurement noise $\mathbf{v}_k \in \mathbb{R}^{m\times 1}$ is characterized by some unknown non-Gaussian, zero-mean, heavy-tailed distribution. The process noise $\mathbf{w}_k$ and measurement noise $\mathbf{v}_k$ are independent of each other and uncorrelated in time. This assumption is adopted for analytical tractability and is commonly used in recursive filtering formulations; however, in practice, certain error sources (e.g., multipath) likely exhibit time-varying temporal correlation.

Because the measurement noise $\mathbf{v}_k$ is no longer Gaussian, conventional Kalman-filter-based PNT filters are not applicable. Therefore, an alternative recursive filter capable of accommodating non-Gaussian noise characteristics is needed. Bayesian inference provides a statistical framework for estimating the *a posteriori* PDF of $\mathbf{x}_k$, given measurements $\mathbf{y}_1, \mathbf{y}_2, \cdots, \mathbf{y}_k$ (Simon, 2006). Free from the assumption of Gaussian noise, Bayesian inference is well-suited for propagating the non-Gaussian overbound. The equations for computing the *a priori* and *a posteriori* PDFs are expressed as follows:

$$\mathbf{P}\left(\mathbf{x}_k \mid \mathbf{Y}_{k-1}\right) = \int \mathbf{P}\left(\mathbf{x}_k \mid \mathbf{x}_{k-1}\right) \mathbf{P}\left(\mathbf{x}_{k-1} \mid \mathbf{Y}_{k-1}\right) d\mathbf{x}_{k-1} \tag{18a}$$

$$P\left(\mathbf{x}_k \mid \mathbf{Y}_k\right) = \frac{\mathbf{P}\left(\mathbf{y}_k \mid \mathbf{x}_k\right) \mathbf{P}\left(\mathbf{x}_k \mid \mathbf{Y}_{k-1}\right)}{\int \mathbf{P}\left(\mathbf{y}_k \mid \mathbf{x}_k\right) \mathbf{P}\left(\mathbf{x}_k \mid \mathbf{Y}_{k-1}\right) d\mathbf{x}_k} \tag{18b}$$

where $\mathbf{Y}_k$ is a collective notation representing the sequence of measurements up to and including the current time step k, i.e., $\mathbf{Y}_k = \{\mathbf{y}_1, \mathbf{y}_2, \cdots, \mathbf{y}_k\}$. $\mathbf{P}\left(\mathbf{x}_k \mid \mathbf{x}_{k-1}\right)$ denotes the Markov transition density. $\mathbf{P}\left(\mathbf{x}_{k-1} \mid \mathbf{Y}_{k-1}\right)$ represents the *a posteriori* PDF at the previous time step $k-1$. $\mathbf{P}\left(\mathbf{y}_k \mid \mathbf{x}_k\right)$ is the likelihood function, and $\mathbf{P}\left(\mathbf{x}_k \mid \mathbf{Y}_{k-1}\right)$ denotes the *a priori* PDF at time step k. Equations (18a) and (18b) can be used to compute the *a priori* and *a posteriori* PDFs of the state vector $\mathbf{x}_k$.

Let us assume that the process noise distribution is perfectly known to us, but the measurement noise $\mathbf{v}_k$ is characterized by some unknown, zero-mean, heavy-tailed distribution. Based on the approaches proposed in Sections 2 and 3, a Gaussian–Pareto distribution can be developed to overbound the unknown heavy-tailed measurement noise distribution. Subsequently, a GMM can be estimated that best fits

the Gaussian–Pareto distribution, while also overbounding the unknown measurement noise distribution. We express the PDF of the estimated conservative GMM for the measurement noise $\mathbf{v}_k$ as follows:

$$\mathbf{P}(\mathbf{v}_k) = \sum_{i=1}^{n_v} \lambda_i \mathcal{N}(\mathbf{v}_k \mid \boldsymbol{\mu}_i, \mathbf{R}_i) = \sum_{i=1}^{n_v} \lambda_i \frac{1}{(2\pi)^{m/2} |\mathbf{R}_i|^{1/2}} \exp\left\{-\frac{1}{2}(\mathbf{v}_k - \boldsymbol{\mu}_i)^T \mathbf{R}_i^{-1}(\mathbf{v}_k - \boldsymbol{\mu}_i)\right\} \tag{19}$$

where n_v is the number of Gaussian mixture components and $\lambda_i, \boldsymbol{\mu}_\mathbf{i}$, and $\mathbf{R}_i$ denote the weight, mean, and covariance matrix, respectively, for the i-th Gaussian component. Thus, Equation (19) can be used in conjunction with Equations (18a) and (18b) to propagate the GMM density in the Bayesian estimator. The type of Bayesian filter that utilizes a GMM for the noise distribution is known as the Gaussian sum filter (Frühwirth, 1997). More details of the Gaussian sum filter can be found in the works by Mahler (2007) and Alspach and Sorenson (1972). Next, we proceed to discuss how the *a priori* and *a posteriori* PDFs are derived in this overbounding filter from the perspective of Bayesian inference.

Time Update: We first derive the time update equation, which leads to the *a priori* PDF of the state estimate. We denote the *a posteriori* PDF of the state vector $\mathbf{x}_{k-1}$ at time step $k-1$ by the following:

$$\mathbf{P}(\mathbf{x}_{k-1} \mid \mathbf{Y}_{k-1}) = \sum_{i=1}^{n_{k-1}} \zeta_i \mathcal{N}(\mathbf{x}_{k-1} \mid \hat{\mathbf{x}}_{i,k-1}^{+}, \mathbf{P}_{i,k-1}^{+}) \tag{20}$$

where n_{k-1} is the number of Gaussian components in $\mathbf{P}(\mathbf{x}_{k-1} \mid \mathbf{Y}_{k-1})$. ζ_i, $\hat{\mathbf{x}}_{i,k-1}^{+}$, and $\mathbf{P}_{i,k-1}^{+}$ are the corresponding weight, mean, and covariance matrix of the i-th Gaussian mixture component, respectively. Using Equation (18a), we can propagate the *a posteriori* PDF $\mathbf{P}(\mathbf{x}_{k-1} \mid \mathbf{Y}_{k-1})$ from time step $k-1$ to k, yielding the *a priori* PDF of $\mathbf{x}_k$ as follows:

$$\begin{aligned}
\mathbf{P}(\mathbf{x}_k \mid \mathbf{Y}_{k-1}) &= \int \mathbf{P}(\mathbf{x}_k \mid \mathbf{x}_{k-1}) \mathbf{P}(\mathbf{x}_{k-1} \mid \mathbf{Y}_{k-1}) d\mathbf{x}_{k-1} \\
&= \int \mathcal{N}(\mathbf{x}_k \mid \mathbf{A}_k \mathbf{x}_{k-1}, \mathbf{Q}_{k-1}) \sum_{i=1}^{n_{k-1}} \zeta_i \mathcal{N}(\mathbf{x}_{k-1} \mid \hat{\mathbf{x}}_{i,k-1}^{+}, \mathbf{P}_{i,k-1}^{+}) d\mathbf{x}_{k-1} \\
&= \sum_{i=1}^{n_{k-1}} \zeta_i \mathcal{N}(\mathbf{x}_k \mid \mathbf{A}_k \hat{\mathbf{x}}_{i,k-1}^{+}, \mathbf{A}_k \mathbf{P}_{i,k-1}^{+} \mathbf{A}_k^T + \mathbf{Q}_{k-1})
\end{aligned} \tag{21}$$

Measurement Update: The derivation of the *a posteriori* PDF equation is more complex than that for the *a priori* PDF, as it involves two distinct cases. The first case occurs when the first measurement arrives, for instance, at time step j. In this case, the likelihood PDF $\mathbf{P}(\mathbf{y}_j \mid \mathbf{x}_j)$ is represented by a GMM, whereas the *a priori* PDF $\mathbf{P}(\mathbf{x}_j \mid \mathbf{Y}_{j-1})$ is Gaussian. The second case arises after the first measurement update, where both $\mathbf{P}(\mathbf{y}_j \mid \mathbf{x}_j)$ and $\mathbf{P}(\mathbf{x}_j \mid \mathbf{Y}_{j-1})$ are modeled as GMMs. Therefore, the computation of the *a posteriori* PDF differs between these two cases. We will first examine case 1.

Case 1: $\mathbf{P}(\mathbf{x}_k \mid \mathbf{Y}_{k-1})$ is a Gaussian distribution, and $\mathbf{P}(\mathbf{y}_k \mid \mathbf{x}_k)$ takes the form of a GMM:

$$\mathbf{P}(\mathbf{y}_k \mid \mathbf{x}_k) = \sum_{j=1}^{n_v} \lambda_j \mathcal{N}(\mathbf{y}_k \mid \mathbf{H}_k \mathbf{x}_k + \boldsymbol{\mu}_j, \mathbf{R}_j) \quad \text{and} \quad \mathbf{P}(\mathbf{x}_k \mid \mathbf{Y}_{k-1}) = \mathcal{N}(\mathbf{x}_k \mid \hat{\mathbf{x}}_k^{-}, \mathbf{P}_k^{-}) \tag{22}$$

The *a posteriori* PDF of $\mathbf{x}_k$ is as follows:

$$\begin{aligned}\mathbf{P}\left(\mathbf{x}_k \mid \mathbf{Y}_k\right) &= \frac{\sum_{j=1}^{n_v} \lambda_j \mathcal{N}\left(\mathbf{y}_k \mid \mathbf{H}_k\mathbf{x}_k + \boldsymbol{\mu}_j, \mathbf{R}_j\right)\mathcal{N}\left(\mathbf{x}_k \mid \hat{\mathbf{x}}_k^-, \mathbf{P}_k^-\right)}{\int \sum_{j=1}^{n_v} \lambda_j \mathcal{N}\left(\mathbf{y}_k \mid \mathbf{H}_k\mathbf{x}_k + \boldsymbol{\mu}_j, \mathbf{R}_j\right)\mathcal{N}\left(\mathbf{x}_k \mid \hat{\mathbf{x}}_k^-, \mathbf{P}_k^-\right)d\mathbf{x}_k} \\ &= \sum_{j=1}^{n_v} \xi_j \mathcal{N}\left(\mathbf{x}_k \mid \hat{\mathbf{e}}_j^+, \mathbf{E}_j^+\right)\end{aligned} \tag{23}$$

where:

$$\begin{aligned}\xi_j &= \frac{\lambda_j \mathcal{N}\left(\mathbf{y}_k^j \mid \mathbf{H}_k\hat{\mathbf{x}}_k^-, \mathbf{R}_j + \mathbf{H}_k\mathbf{P}_k^-\mathbf{H}_k^T\right)}{\sum_{j=1}^{n_v} \lambda_j \mathcal{N}\left(\mathbf{y}_k^j \mid \mathbf{H}_k\hat{\mathbf{x}}_k^-, \mathbf{R}_j + \mathbf{H}_k\mathbf{P}_k^-\mathbf{H}_k^T\right)} & \mathbf{y}_k^j &= \mathbf{y}_k - \boldsymbol{\mu}_j \\ \hat{\mathbf{e}}_j^+ &= \mathbf{E}_j^+((\mathbf{P}_k^-)^{-1}\hat{\mathbf{x}}_k^- + \mathbf{H}_k^T(\mathbf{R}_j)^{-1}\mathbf{y}_k^j) & \mathbf{E}_j^+ &= ((\mathbf{P}_k^-)^{-1} + \mathbf{H}_k^T(\mathbf{R}_j)^{-1}\mathbf{H}_k)^{-1}\end{aligned} \tag{24}$$

Case 2: Both $\mathbf{P}\left(\mathbf{x}_k \mid \mathbf{Y}_{k-1}\right)$ and $\mathbf{P}\left(\mathbf{y}_k \mid \mathbf{x}_k\right)$ are GMM distributions:

$$\mathbf{P}\left(\mathbf{y}_k \mid \mathbf{x}_k\right) = \sum_{j=1}^{n_v} \lambda_j \mathcal{N}\left(\mathbf{y}_k \mid \mathbf{H}_k\mathbf{x}_k + \boldsymbol{\mu}_j, \mathbf{R}_j\right) \quad \text{and} \quad \mathbf{P}\left(\mathbf{x}_k \mid \mathbf{Y}_{k-1}\right) = \sum_{i=1}^{n_k} \zeta_i \mathcal{N}\left(\mathbf{x}_k \mid \hat{\mathbf{x}}_{i,k}^-, \mathbf{P}_{i,k}^-\right) \tag{25}$$

The *a posteriori* PDF of $\mathbf{x}_k$ is as follows:

$$\begin{aligned}\mathbf{P}(\mathbf{x}_k \mid \mathbf{Y}_k) &= \frac{\sum_{j=1}^{n_v} \lambda_j \mathcal{N}\left(\mathbf{y}_k \mid \mathbf{H}_k\mathbf{x}_k + \boldsymbol{\mu}_j, \mathbf{R}_j\right)\sum_{i=1}^{n_k} \zeta_i \mathcal{N}\left(\mathbf{x}_k \mid \hat{\mathbf{x}}_{i,k}^-, \mathbf{P}_{i,k}^-\right)}{\int \sum_{j=1}^{n_v} \lambda_j \mathcal{N}\left(\mathbf{y}_k \mid \mathbf{H}_k\mathbf{x}_k + \boldsymbol{\mu}_j, \mathbf{R}_j\right)\sum_{i=1}^{n_k} \zeta_i \mathcal{N}\left(\mathbf{x}_k \mid \hat{\mathbf{x}}_{i,k}^-, \mathbf{P}_{i,k}^-\right)d\mathbf{x}_k} \\ &= \sum_{j=1}^{n_v}\sum_{i=1}^{n_k} \xi_{i,j} \mathcal{N}(\mathbf{x}_k \mid \hat{\mathbf{e}}_{i,j}^+, \mathbf{E}_{i,j}^+)\end{aligned} \tag{26}$$

where:

$$\begin{aligned}\xi_j &= \frac{\lambda_j \zeta_i \mathcal{N}\left(\mathbf{y}_k^j \mid \mathbf{H}_k\hat{\mathbf{x}}_{i,k}^-, \mathbf{R}_j + \mathbf{H}_k\mathbf{P}_{i,k}^-\mathbf{H}_k^T\right)}{\sum_{j=1}^{n_v}\sum_{i=1}^{n_k} \lambda_j \zeta_i \mathcal{N}\left(\mathbf{y}_k^j \mid \mathbf{H}_k\hat{\mathbf{x}}_{i,k}^-, \mathbf{R}_j + \mathbf{H}_k\mathbf{P}_{i,k}^-\mathbf{H}_k^T\right)} & \mathbf{y}_k^j &= \mathbf{y}_k - \boldsymbol{\mu}_j \\ \hat{\mathbf{e}}_{i,j}^+ &= \mathbf{E}_{i,j}^+((\mathbf{P}_{i,k}^-)^{-1}\hat{\mathbf{x}}_{i,k}^- + \mathbf{H}_k^T(\mathbf{R}_j)^{-1}\mathbf{y}_k^j) & \mathbf{E}_{i,j}^+ &= ((\mathbf{P}_{i,k}^-)^{-1} + \mathbf{H}_k^T(\mathbf{R}_j)^{-1}\mathbf{H}_k)^{-1}\end{aligned} \tag{27}$$

Equations (21), (23), and (26) comprise the major steps of the recursive Bayesian overbounding filter. With this, we now have a recursive navigation filter capable of taking as input a GMM overbound of the unknown non-Gaussian measurement noise and propagating the PDF of the state estimate forward with time. Importantly, under the assumption that the measurement noise model is a conservative overbound of the corresponding true distributions, the *a posteriori* state distribution produced at each recursion is also intended to remain a conservative overbound of the unknown true state error distribution. This property is preserved through successive time and measurement updates because both updates can be interpreted as convolution operations and, according to DeCleene (2000) and Larson et al. (2019a), convolution of unbiased, symmetric, and unimodal overbounding distributions yields an overbound of the output distribution. As a result, the full posterior GMM obtained at each time step is treated as an overbounding

model for integrity monitoring. However, it is worth noting that the number of Gaussian mixture components in the *a posteriori* PDF increases with each measurement update. For instance, the *a posteriori* PDF in Equation (26) will contain 10,000 Gaussian terms if $n_v = 100$ and $n_k = 100$. These 10,000 terms will compound into the *a posteriori* PDF at the next measurement update, causing rapid growth in the number of Gaussian mixture components, which could lead to significant computational burdens and limit the practicality of the filter.

Possible workarounds for alleviating this issue have been discussed by Sorenson and Alspach (1971) and Alspach and Sorenson (1972), who suggested either merging similar terms or discarding terms with sufficiently small weights. While these approaches can effectively prevent rapid growth of the Gaussian components, they may potentially undermine the primary objective of this work, which is to ensure the overbounding of system output errors for safety-critical systems. The tails of the state estimate distribution are particularly sensitive to even small changes in the Gaussian mixture components. Merging or discarding terms could significantly alter the overbounding performance in the tails, thereby compromising the integrity monitoring of the navigation system. Therefore, an alternative strategy to address the growth of Gaussian components is required to reduce the computational load while preserving conservatism.

Inspired by the approach proposed in Section 3 for developing a conservative GMM that best fits the Gaussian–Pareto overbound, we introduce a similar strategy to address the issue of term growth in the GMMs of the *a posteriori* density. Specifically, given the *a posteriori* PDF with a large number of Gaussian mixture components, we propose fitting a new GMM to the PDF but with much fewer components. Meanwhile, the constraints in Equation (13) ensure that the new GMM can still overbound the true underlying distribution. Additionally, it is worth noting that this GMM term-trimming approach is performed using the conservative GMM estimation formulation in Equation (13), which enforces overbounding over a finite, specified range that is relevant to integrity monitoring. Outside this range, the fit is neither optimized nor constrained. Figure 10 illustrates the proposed GMM term-trimming approach. The original GMM (red solid) consists of 2000 Gaussian mixture components. To reduce the number of Gaussian components in the original GMM, a new GMM (blue dashed) with only 200 Gaussian components is derived to best fit the original GMM by applying the conservative GMM estimation approach described in Section 3. The fitting performance, particularly in the tails of the distribution, is highlighted in Figures 10(b) and (c). As shown, the new GMM closely approximates the original GMM. Thereby, the original GMM with 2000 Gaussian terms can be effectively replaced by the new GMM with only

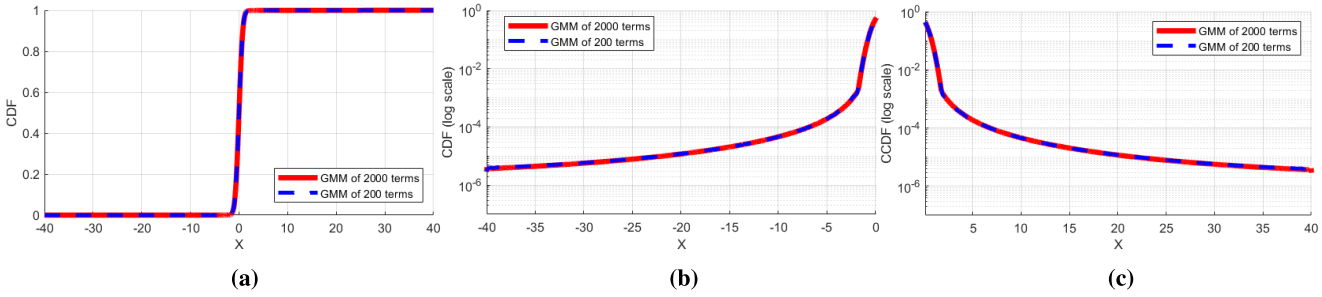

FIGURE 10 (a) Comparison of the CDFs of two GMMs: one containing 2000 Gaussian mixture components (red solid) and one containing 200 Gaussian mixture components (blue dashed); (b) zoomed-in view of the left-hand tails on a logarithmic scale; (c) zoomed-in view of the right-hand tails on a logarithmic scale

200 terms, while retaining its conservative overbounding properties. That is, if the original GMM overbounds the true underlying distribution, the reduced GMM also overbounds it but with far fewer Gaussian terms. Consequently, this term-trimming approach mitigates the exponential growth of GMM terms in the *a posteriori* density within the recursive Bayesian filter, avoiding the potential computational burden caused by exponential term growth.

5 | SIMULATION CASE STUDY

A simulation case study was conducted to validate the efficacy of the proposed algorithm. In this study, we focus on the fault-free integrity of an airplane approach and landing. During the approach and landing phase of flight, airplanes operate in proximity to terrain, obstacles, and other aircraft. Thus, the integrity of the approach and landing systems is particularly critical for ensuring safety during this vital phase of flight. The radar altimeter is a low-power radar system that measures the distance between the aircraft and the terrain directly beneath it, providing above-ground-level (AGL) height data. This system is frequently utilized by commercial aircraft during approach and landing operations and is typically integrated as part of the aircraft's air data system. Its precise altitude measurements enhance situational awareness, improve approach stability, and contribute to the overall safety and reliability of navigation during critical flight phases.

Figure 11 illustrates the approach and landing of a commercial airplane. The radar altimeter is typically mounted on the underside of the fuselage. It determines the distance to the terrain surface by measuring the time it takes for the radio signal to travel from the aircraft to the ground and back. The time measurement is used to calculate the AGL altitude, which is a critical parameter for low-altitude flight, particularly during approach and landing operations.

In this case study, we focus on the integrity of the aircraft's vertical positioning during the approach and landing phase of the flight. The aircraft is assumed to follow a stabilized approach to landing. The glide path maintains a constant 3° to the touchdown zone on the runway. A light general-aviation aircraft usually descends at 500 ~ 1000 feet per minute (fpm) for a stabilized approach (Federal Aviation

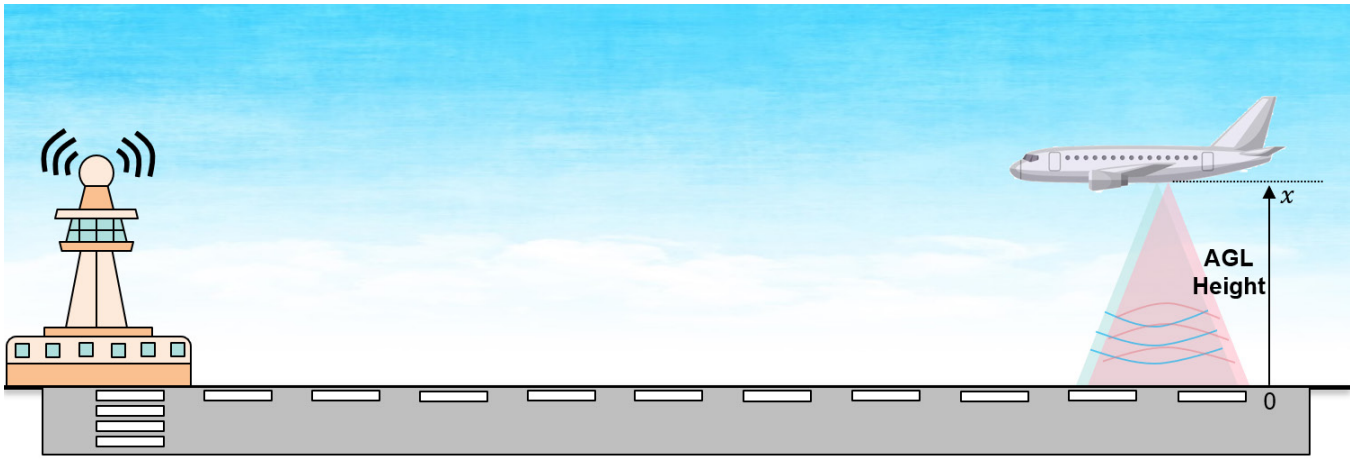

FIGURE 11 Illustration of an airplane approach and landing
The radar altimeter can measure the AGL height of the airplane, by measuring the time delay between the transmitted signal and the reflected signal to determine the distance to the target.

Administration, 2022). The radar altimeter measures the AGL height of the aircraft. The altitude accuracy of civil- and commercial-grade radar altimeters typically ranges from 1.5 to 3 feet (Frick, n.d.). In this case study, we chose 1.5 feet as the altitude accuracy of the radar altimeter sensor. The system and measurement equations of the descending aircraft along the vertical direction can be expressed as follows:

$$x_k = x_{k-1} + u_{k-1}\Delta T + w_{k-1} \tag{28a}$$

$$y_k = x_k + v_k \tag{28b}$$

Equation (28a) describes the system dynamics, where x_k represents the vertical position of the aircraft at time step k, as illustrated in Figure 11. The control input u_k denotes the descent velocity. For this simulation, we assume a constant descent rate with a nominal value $u_k = -500$ fpm (≈ -2.5 m/s), following the stabilized approach criteria outlined by the Federal Aviation Administration (2022). However, the descent velocity information is affected by stochastic noise, and the term w_{k-1} in Equation (28a) represents the uncertainty introduced by the imperfect descent velocity information. The process noise w_k is modeled as a zero-mean, temporally uncorrelated Gaussian process with a standard deviation of $\sigma_w = 0.5$ m. The sampling period is set as $\Delta T = 0.1$ s for this simulation. The assumption of temporally uncorrelated process noise at this rate is adopted for analytical tractability; however, in practice, certain error sources may exhibit temporal correlation. Equation (28b) represents the measurement model, where y_k is the radar altimeter's measured altitude and v_k denotes the measurement noise, which is set to some non-Gaussian, zero-mean, heavy-tail distribution. For this simulation, we use a Student's t distribution to simulate the heavy-tail measurement noise v_k. The standard deviation of v_k is set to 0.45 m ($\approx$ 1.5 feet). Radar altimeter altitude measurements are available every 10 time steps, and the initial altitude is set to $x_0 = 45$ m.

Following the process outlined in Algorithm 1, the first step is to develop overbounds for the unknown sensor error v_k. A total of 5×10^6 samples are drawn from the sensor error distribution, which is a heavy-tailed Student's t distribution in this simulation. Using the method described in Section 2, a CDF interval encompassing the true sensor error CDF is constructed with a specified level of confidence based on the DKW inequality. Subsequently, both Gaussian–Pareto and Gaussian distributions are derived to overbound the CDF interval, thereby providing a conservative overbound for the true underlying error distribution.

The parameters of the Gaussian–Pareto overbound are summarized in Table 3. The Gaussian overbound, in contrast, has zero mean and a standard deviation of $\sigma = 3.7638$ m. Figure 12(a) shows the CDFs of the Gaussian–Pareto and Gaussian distributions developed to overbound the radar altimeter measurement error v_k. Figures 12(b) and (c) highlight the left-hand and right-hand tails, respectively. It can be seen that both the Gaussian–Pareto (blue dashed) and Gaussian (cyan dotted) distributions can overbound the CDF interval (yellow region), which itself encompasses the true CDF (black dashed) with 95% confidence. Moreover, within the probability range covered by the empirical CDF constructed from the sampled data, the Gaussian–Pareto distribution provides a significantly tighter overbound than the Gaussian distribution. It is important to note that, at sufficiently low probabilities beyond the plotted range, the Gaussian overbound—owing to its exponentially decaying tails—can indeed become tighter than the Gaussian–Pareto overbound and may eventually violate the DKW-derived CDF interval (yellow region). In this work, the overbounding requirement is enforced over a finite, integrity-relevant

TABLE 3
Variables of the Gaussian–Pareto Overbound for the Radar Altimeter Error Distribution

Left-hand Tail Threshold u_{L}	−2.0627	**Right-hand Tail Threshold** u_{R}	2.0627
Left-hand Tail GPD $\hat{\gamma}'_{\mathrm{L}}$	0.5817	**Right-hand Tail GPD** $\hat{\gamma}'_{\mathrm{R}}$	0.5817
Left-hand Tail GPD $\hat{\beta}'_{\mathrm{L}}$	0.8634	**Right-hand Tail GPD** $\hat{\beta}'_{\mathrm{R}}$	0.8634
Core Mean μ	0	**Core Standard Deviation** σ	0.7103

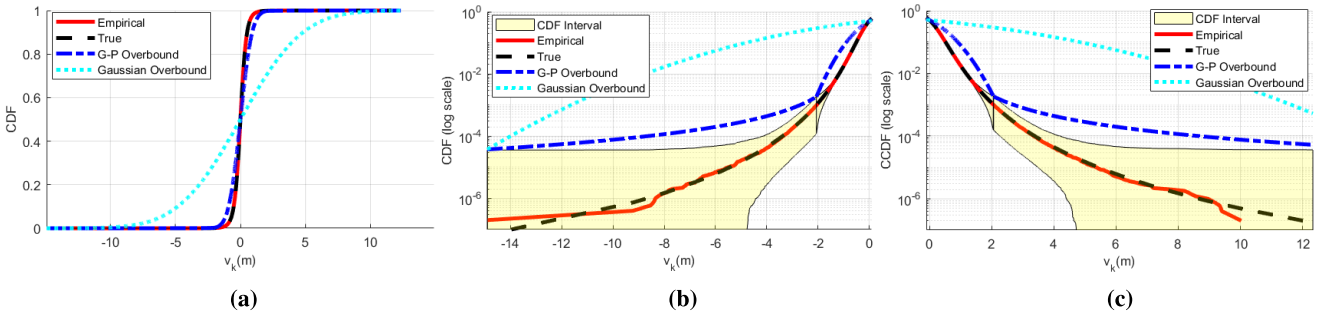

FIGURE 12 (a) The CDFs of the Gaussian–Pareto overbound (blue dashed) and the Gaussian overbound (cyan dotted) compared with the true and empirical distributions of the radar altimeter measurement error v_k; (b) CDFs for the left-hand tails of the Gaussian–Pareto and Gaussian overbounds, where the confidence level of overbounding the CDF interval (yellow region) is 95%; (c) CCDF for the right-hand tails of the Gaussian–Pareto and Gaussian overbounds, where the confidence level of overbounding the CDF interval (yellow region) is 95%

range of the error domain rather than over the entire support of the distribution. Within this specified range, both the Gaussian–Pareto and Gaussian distributions are constructed to conservatively overbound the DKW confidence interval.

Next, we apply the conservative GMM estimation approach described in Section 3 to approximate the Gaussian–Pareto overbound by a conservative GMM that also overbounds the underlying error distribution. We set the number of Gaussian mixture components to $n = 500$. The means of the Gaussian components are evenly spaced within the range [–40, 40]. The shared standard deviation is set to 0.20 m. Figure 13 displays the CDF of the estimated GMM (magenta dash-dotted) along with the Gaussian–Pareto overbound (blue dashed). As shown, the estimated GMM tracks the Gaussian–Pareto very closely and overbounds the CDF interval (yellow region), thereby ensuring that it overbounds the true underlying CDF (black dashed).

The performances of three different PNT filters are compared in this simulation. The first is our proposed recursive Bayesian filter, which utilizes the estimated GMM overbounds as the sensor error input and propagates the density of the system state estimate forward. The second is the conventional Kalman filter, which operates in parallel with the recursive Bayesian filter. The Kalman filter employs the derived Gaussian overbound as the sensor error input and maintains a Gaussian density estimate of the system state at each time step. Lastly, a particle filter is implemented as a benchmark that serves as a reference for the Bayesian filter and Kalman filter for comparison. For this particle filter, a Student's t distribution is used to compute the likelihood density for the particle weight update. Therefore, this particle filter simulates the ideal case in which the sensor noise distribution is perfectly known. However, during the steps of the particle weight update, particles in the distribution tails, which embody significantly large errors, tend to be assigned smaller weights, whereas particles closer to the core (with smaller errors) are updated with larger weights. Consequently, during the importance resampling,

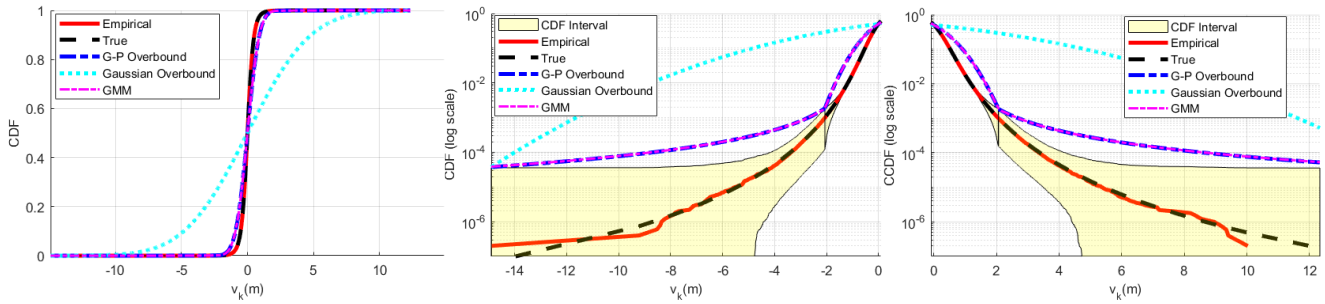

FIGURE 13 (a) CDF of the estimated GMM (magenta dash-dotted) in comparison with the Gaussian–Pareto overbound (blue dashed); (b) CDFs for the left-hand tails of the GMM and Gaussian–Pareto overbound; (c) CCDFs for the right-hand tails of the GMM and Gaussian–Pareto overbounds
In (a), the GMM almost overlaps with the Gaussian–Pareto overbound and can overbound the CDF interval (yellow region), thereby overbounding the true underlying error distribution.

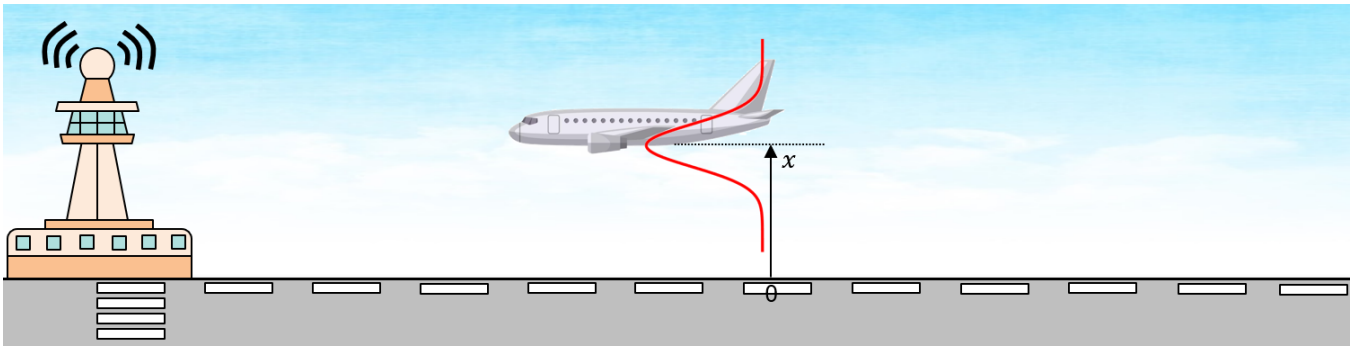

FIGURE 14 During aircraft approach and landing, the behavior of the vertical position distribution's tail near the ground is of critical concern.

particles with large weights have a higher probability of being resampled, whereas particles with smaller weights are more likely to be discarded. This leads to potential alterations in the tails of the state estimate density due to the loss of particles during the importance resampling step, which indicates that the fidelity of the tails of the state estimate density could potentially be compromised for the particle filter. To maintain reasonable accuracy in the tails of the state estimate density, increasing the particle population is a viable approach. In this simulation, the particle population is set to 1×10^7 to ensure that the particle filter adequately captures the state estimate density, particularly in the tails.

As shown in Figure 14, during the aircraft approach and landing, the behavior of the vertical position distribution's tail near the ground is of critical concern, as the tail near the ground represents extreme deviations from the nominal vertical position, which could potentially result in severe consequences, e.g., controlled flight into terrain, thereby directly impacting the safety of landing operations. To prevent potential terrain conflicts and ensure landing safety, timely warnings must be issued to alert the pilot whenever the vertical position error exceeds the prescribed alert limit for the tail near the ground. The vertical protection level (VPL) is the statistical bound on the vertical positioning errors, which ensures that the aircraft maintains a safe altitude above terrain and obstacles. When the protection level exceeds the prescribed alert limit, the PNT system raises an alert, warning users that the navigation data cannot be trusted.

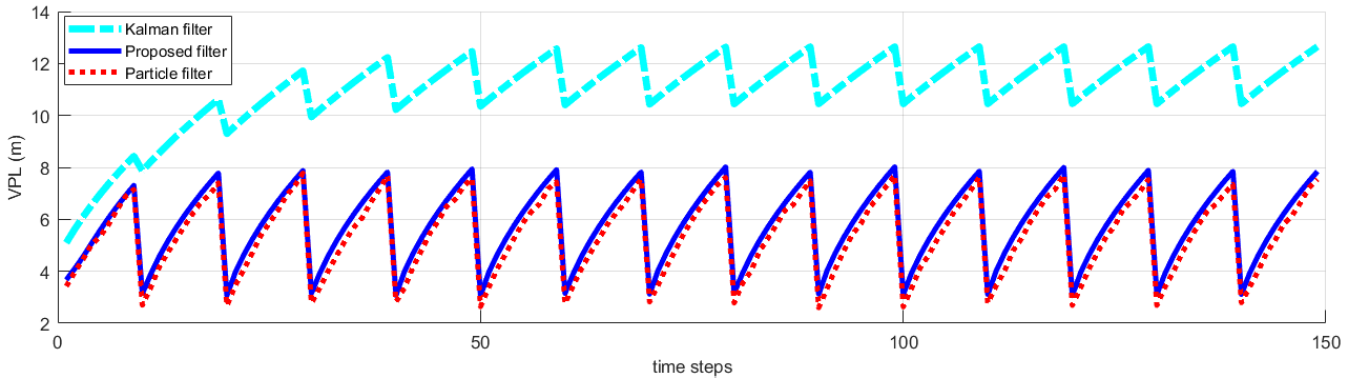

FIGURE 15 Comparison of VPLs for the three different PNT filters
Compared with the conventional Kalman filter (cyan dash-dotted), our proposed recursive Bayesian filter (blue solid) using the Gaussian–Pareto overbound can achieve smaller VPLs, which indicates increased availability of the PNT system. Additionally, the VPLs of our proposed algorithm can consistently bound those of the benchmark particle filter (red dotted).

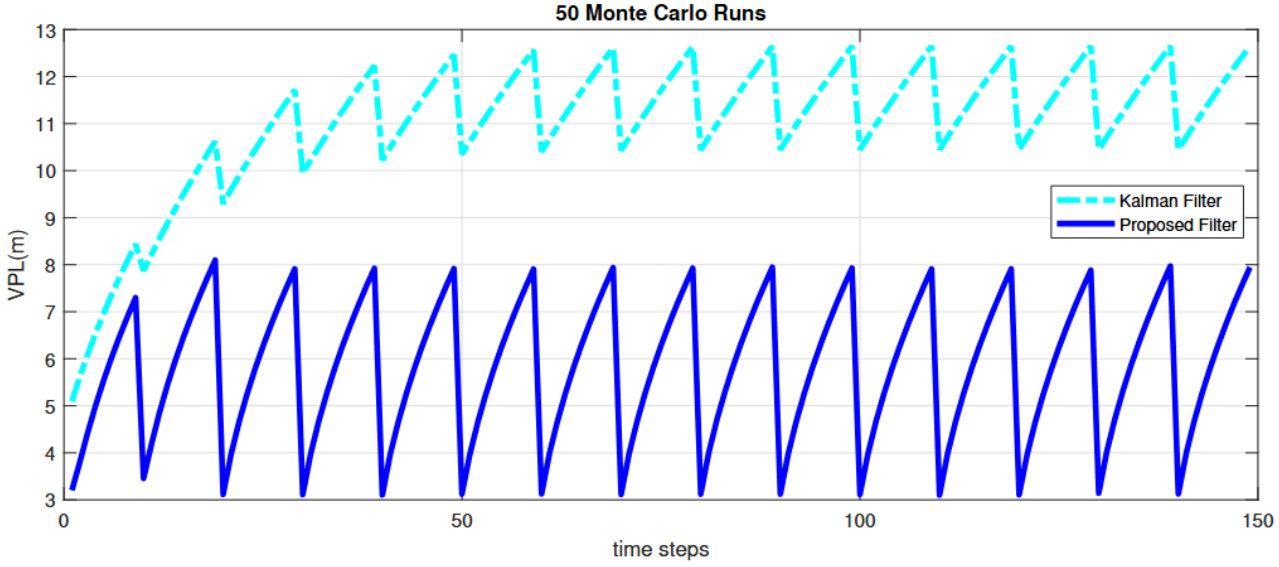

FIGURE 16 Comparison of average VPLs of the conventional Kalman filter (cyan dash-dotted) and the proposed recursive Bayesian overbounding filter (blue solid) over 50 MC simulation runs

In this simulation, we set the integrity risk to 10^{-6}. Accordingly, the VPLs can be calculated for each PNT filter at each time step. For the proposed recursive Bayesian filter, we keep track of the full state estimate density at each time step. This allows the VPLs to be determined by calculating the vertical position errors corresponding to the prescribed integrity risk on the tail of the CDF of the state estimate error. Similarly, the VPLs for the Kalman filter and the particle filter can be computed using the same approach. Figure 15 presents the VPLs of the tail near the ground for the three different PNT filters corresponding to an integrity risk of 1×10^{-6} during the approach and landing phase. It can be seen that our proposed algorithm (blue solid) can achieve smaller VPLs than the conventional Kalman filter (cyan dash-dotted), which indicates that our proposed algorithm can increase the availability of the PNT system. Additionally, the VPLs of our proposed algorithm consistently bound the VPLs computed by the benchmark particle filter

(red dotted), which assumes perfect knowledge of the radar altimeter error distribution. The VPL results of the simulation demonstrate that our proposed recursive Bayesian overbounding filter using Gaussian–Pareto distributions can effectively overbound the system output errors while achieving higher availability than the conventional Gaussian overbounding methods.

Additionally, 50 MC simulation runs were performed, and the average VPLs for both the conventional Kalman filter and the proposed recursive Bayesian overbounding filter are illustrated in Figure 16. The MC simulation results further demonstrate that the proposed recursive Bayesian overbounding filter consistently achieves smaller VPLs, indicating improved availability of the navigation system compared with the conventional Kalman filter.

6 | DISCUSSION ON NONLINEAR AND MULTIVARIATE EXTENSIONS

The proposed recursive Bayesian overbounding filter using a Gaussian–Pareto distribution was assessed using a one-dimensional linear PNT problem in Section 5. However, practical PNT systems are more complex, often involving nonlinearity and higher dimensionality. For instance, in global navigation satellite system (GNSS) positioning, the measurement equations are inherently nonlinear, and the dimensionality depends on the number of GNSS satellites visible at a given time. Inertial navigation is also a multidimensional nonlinear problem owing to the nonlinearity introduced by coordinate transformation and the multivariate state vector. While the recursive Bayesian overbounding filter in Section 4 was derived for a multidimensional linear system, extensions to nonlinear systems are possible via linearization, as shown by Alspach and Sorenson (1972). However, a key limitation arises when the measurement noise is multivariate. The Gaussian–Pareto overbounding technique relies on the univariate EVT. However, this univariate EVT cannot be directly extended to multivariate cases, as the concepts defined in the univariate extreme value analysis lose their evident definition in the multivariate context. For example, the definition of a tail for a multivariate distribution is problematic (Dutfoy et al., 2014): is it sufficient for just one single entry to approach an extreme value or should the tail refer to the case in which extreme values are attained in all dimensions? Additionally, the dependence structure of the joint tail distribution poses another challenge for estimating the multivariate probabilities of extreme risks. Thus, the Gaussian–Pareto overbounding approach is inadequate for modeling a multivariate overbound when the measurement noise is a vector.

Nevertheless, a solution exists for cases in which the entries of the measurement noise vector are independent of each other. In such cases, the dependence structure of the joint tail distribution is trivial, and the multivariate overbounding problem can be simplified by independently overbounding each coordinate. For instance, given a measurement vector $\mathbf{y} = [y_1 \quad y_2 \quad \dots \quad y_m]$, where each entry $\mathbf{y}_i$ is independent of each other, applying a measurement update using the vector $\mathbf{y}$ is equivalent to a sequential measurement update using each scalar entry y_i. By means of the sequential measurement update scheme, we are able to transform the measurement vector into a sequence of univariate measurements. Thereby, the Gaussian–Pareto overbounding approach can be applied individually to each coordinate. However, when the entries of the measurement noise vector are correlated and the dependence structure of the joint tail cannot be ignored, this sequential measurement update scheme is no longer valid. This limitation highlights the need for more advanced multivariate overbounding techniques to address correlated measurement errors. McNeil (1999), Dupuis and Jones (2006), and Dutfoy et al.

(2014) studied the multivariate EVT, which considers the modeling of tails for multivariate distributions. Rife (2018) and J. Larson et al. (2019b) tackled multivariate overbounding from a different perspective. Through coordinate transformation and probability marginalization, the original multivariate distribution can be marginalized into separate angular distributions and radial distributions. Univariate overbounding techniques can be applied to the angular and radial distributions independently. These approaches provide a foundation for extending the proposed algorithm to accommodate more complex PNT problems that involve multivariate and correlated measurement noise. Addressing these challenges will be a valuable focus for future research.

7 | CONCLUSION

In this paper, we proposed a recursive Bayesian overbounding filter that utilizes the Gaussian–Pareto distribution to overbound the input measurement noise and can ensure bounded tail probabilities of the system output errors for safety-critical PNT systems. The contributions of the proposed filter are as follows: (1) the use of the DKW inequality to reliably determine the Gaussian–Pareto overbounds with a quantifiable measure of confidence in overbounding the true, typically unknown, underlying distribution, (2) a nonlinear least-square-based GMM estimation approach to best fit the Gaussian–Pareto overbound while maintaining the advantageous convolutional properties of Gaussian distributions, and (3) a recursive Bayesian filter for efficient overbound propagation integrated with a culling algorithm that mitigates the exponential growth of Gaussian mixture terms, ensuring computational tractability without compromising the conservativeness of the bounds. A simulation example of an aircraft approach and landing was conducted to validate the proposed algorithm. The simulation results show that our proposed algorithm achieves smaller VPLs compared with the traditional Gaussian overbounding approach, demonstrating that our proposed algorithm can achieve increased availability for PNT systems.

Furthermore, the VPLs computed by the proposed algorithm consistently bound those computed by the benchmark particle filter, indicating that the proposed algorithm effectively overbounds the system output errors. Additionally, the limitations of the proposed algorithm were discussed at the end of this paper. The Gaussian–Pareto overbounding technique, based on univariate EVT, is only applicable to scalar random variables. The sequential measurement update scheme enables the Gaussian–Pareto overbounding method to be applied to multivariate PNT problems, provided that the entries of the measurement vector are independent of each other. Nevertheless, a multivariate overbounding approach is still required for PNT problems when the dependence structure of the joint tail of the measurement vector cannot be ignored. Therefore, an important direction for future work will focus on extending the Gaussian–Pareto overbounding technique to multivariate scenarios and applying the Bayesian overbounding filter to multidimensional, nonlinear stochastic systems. Additionally, while the DKW inequality provides a rigorous, distribution-free confidence bound under finite data and limited prior knowledge, its uniform confidence interval can introduce additional conservatism, particularly in the distribution tails. Another important direction for future work is exploring the possibility of incorporating additional structural assumptions or alternative statistical tools that yield tighter, non-uniform confidence bounds—particularly in the tails, to significantly reduce conservatism while preserving integrity guarantees.

ACKNOWLEDGMENTS

The authors would like to thank and acknowledge the Center for Transportation Studies (CTS) and the College of Science and Engineering (CSE) at the University of Minnesota which provided funding support for the work reported in this paper.

REFERENCES

Alspach, D., & Sorenson, H. (1972). Nonlinear Bayesian estimation using Gaussian sum approximations. *IEEE Transactions on Automatic Control*, *17*(4), 439–448. https://doi.org/10.1109/TAC.1972.1100034

Blanch, J., Walter, T., & Enge, P. (2008). Position error bound calculation for GNSS using measurement residuals. *IEEE Transactions on Aerospace and Electronic Systems*, *44*(3), 977–984. https://ieeexplore.ieee.org/document/4655357

Blanch, J., Walter, T., & Enge, P. (2018). Gaussian bounds of sample distributions for integrity analysis. *IEEE Transactions on Aerospace and Electronic Systems*, *55*(4), 1806–1815. https://doi.org/10.1109/TAES.2018.2876583

Blanch, J., Walter, T., Enge, P., Lee, Y., Pervan, B., Rippl, M., & Spletter, A. (2012, September). Advanced RAIM user algorithm description: Integrity support message processing, fault detection, exclusion, and protection level calculation. In *Proceedings of the 25th International Technical Meeting of the Satellite Division of the Institute of Navigation (ION GNSS 2012)* (pp. 2828–2849). https://www.ion.org/publications/abstract.cfm?articleID=10462

DeCleene, B. (2000, September). Defining pseudorange integrity-overbounding. In *13th International Technical Meeting of the Satellite Division of the Institute of Navigation (ION GPS 2000)* (pp. 1916–1924). https://www.ion.org/publications/abstract.cfm?articleID=1603

Dupuis, D., & Jones, B. (2006). Multivariate extreme value theory and its usefulness in understanding risk. *North American Actuarial Journal*, *10*(4), 1–27. https://doi.org/10.1080/10920277.2006.10597411

Dutfoy, A., Parey, S., & Roche, N. (2014). Multivariate extreme value theory-A tutorial with applications to hydrology and meteorology. *Dependence Modeling*, *2*(1), 30–48. https://doi.org/10.2478/demo-2014-0003

European Space Agency. (2025). Integrity. In *Navipedia*. Retrieved December 21, 2025, from https://gssc.esa.int/navipedia/index.php/Integrity#cite_note-Annex10-3

Federal Aviation Administration. (2022). *Airplane flying handbook: FAA-H-8083-3C (2024)*. Simon and Schuster.

Federal Aviation Administration. (2023, September). *FAA order 8040.4c safety risk management policy*. U.S. Department of Transportation. Washington, D.C.

Federal Aviation Administration. (2024, August). *System design and analysis advisory circular AC 25.1309-1B*. U.S. Department of Transportation. Washington, D.C.

Frick, S. (n.d.). *Radar altimeters: Overview of operation, design, and performance, year=2021*. Retrieved November 20, 2024, from https://avsi.aero/wp-content/uploads/2021/12/Radar-Altimeter-Overview-of-Design-and-Performance.pdf

Frühwirth, R. (1997). Track fitting with non-Gaussian noise. *Computer Physics Communications*, *100*(1-2), 1–16. https://doi.org/10.1016/S0010-4655(96)00155-5

Hu, Y. (2024, September). Bayesian overbounding filter using Gaussian-Pareto distributions. In *Proceedings of the 37th International Technical Meeting of the Satellite Division of the Institute of Navigation (ION GNSS+ 2024)* (pp. 1785–1799). https://doi.org/10.33012/2024.19865

Larson, J., & Gebre-Egziabher, D. (2017). Conservatism assessment of extreme value theory overbounds. *IEEE Transactions on Aerospace and Electronic Systems*, *53*(3), 1295–1307. https://doi.org/10.1109/TAES.2017.2669838

Larson, J., Gebre-Egziabher, D., & Rife, J. H. (2019a). Gaussian-Pareto overbounding of DGNSS pseudoranges from CORS. *NAVIGATION*, *66*(1), 139–150. https://doi.org/10.1002/navi.276

Larson, J., Gebre-Egziabher, D., & Rife, J. H. (2019b). Multivariate error overbounding with a Gaussian–Pareto model. *Journal of Aerospace Information Systems*, *16*(4), 148–161. https://doi.org/10.2514/1.I010675

Larson, J. (2018). *Gaussian-Pareto overbounding: A method for managing risk in safety-critical navigation systems* [Doctoral dissertation, University of Minnesota].

Lee, J. (2004, September). LAAS position domain monitor analysis and test results for CAT II/III operations. In *Proceedings of the 17th International Technical Meeting of the Satellite Division of the Institute of Navigation (ION GNSS 2004)* (pp. 2786–2796). https://www.ion.org/publications/abstract.cfm?articleID=5962

Mahler, R. (2007). *Statistical multisource-multitarget information fusion*. Artech.

Massart, P. (1990). The tight constant in the Dvoretzky-Kiefer-Wolfowitz inequality. *The Annals of Probability*, *18*(3), 1269–1283.

McNeil, A. J. (1999). Extreme value theory for risk managers. *Departement Mathematik ETH Zentrum*, *12*(5), 217–237.

Pickands, J., III (1975). Statistical inference using extreme order statistics. *The Annals of Statistics*, *3*(1), 119–131. https://doi.org/10.1214/aos/1176343003

Reynolds, D. A. (2009). Gaussian mixture models. *Encyclopedia of Biometrics*, *741*, 659–663. https://doi.org/10.1007/978-0-387-73003-5_196

Rife, J. (2018). Overbounding risk for quadratic monitors with arbitrary noise distributions. *IEEE Transactions on Aerospace and Electronic Systems*, *54*(4), 1618–1627. https://doi.org/10.1109/TAES.2018.2798258

Rife, J., & Gebre-Egziabher, D. (2007). Symmetric overbounding of correlated errors. *NAVIGATION*, *54*(2), 109–124. https://doi.org/10.1002/j.2161-4296.2007.tb00398.x

Rife, J., & Pervan, B. (2012). Overbounding revisited: Discrete error-distribution modeling for safety-critical GPS navigation. *IEEE Transactions on Aerospace and Electronic Systems*, *48*(2), 1537–1551. https://doi.org/10.1109/TAES.2012.6178077

Rife, J., Pullen, S., Enge, P., & Pervan, B. (2006). Paired overbounding for nonideal LAAS and WAAS error distributions. *IEEE Transactions on Aerospace and Electronic Systems*, *42*(4), 1386–1395. https://doi.org/10.1109/TAES.2006.314579

Rife, J., Pullen, S., & Pervan, B. (2004, September). Core overbounding and its implications for LAAS integrity. In *Proceedings of the 17th International Technical Meeting of the Satellite Division of the Institute of Navigation (ION GNSS 2004)* (pp. 2810–2821). https://www.ion.org/publications/abstract.cfm?articleID=5964

Simon, D. (2006). *Optimal state estimation: Kalman, H infinity, and nonlinear approaches*. John Wiley & Sons.

Sorenson, H. W., & Alspach, D. L. (1971). Recursive Bayesian estimation using Gaussian sums. *Automatica*, *7*(4), 465–479. https://doi.org/10.1016/0005-1098(71)90097-5

Walter, T., Hansen, A., & Enge, P. (1999, June). Validation of the WAAS MOPS integrity equation. In *Proceedings of the 55th Annual Meeting of the Institute of Navigation (1999)* (pp. 217–226). https://www.ion.org/publications/abstract.cfm?articleID=10955

Wang, K., El-Mowafy, A., Rizos, C., & Wang, J. (2020). Integrity monitoring for horizontal RTK positioning: New weighting model and overbounding CDF in open-sky and suburban scenarios. *Remote Sensing*, *12*(7), 1173. https://doi.org/10.3390/rs12071173

Yan, P., Zhong, Y., & Hsu, L. T. (2025, February). Principal Gaussian overbound for heavy-tailed error bounding. *IEEE Transactions on Aerospace and Electronic Systems*, *61*(1), 829–852. https://doi.org/10.1109/TAES.2024.3448405

Yun, H., Yun, Y., & Kee, C. (2011). Carrier phase-based RAIM algorithm using a Gaussian sum filter. *The Journal of Navigation*, *64*(1), 75–90. https://doi.org/10.1017/S0373463310000330

Yun, Y., Yun, H., & Kim, C., D.and Kee. (2008). A Gaussian sum filter approach for DGNSS integrity monitoring. *The Journal of Navigation*, *61*(4), 687–703. https://doi.org/10.1017/S0373463308004906

Zhai, Y., Zhan, X., & Pervan, B. (2019). Bounding integrity risk and false alert probability over exposure time intervals. *IEEE Transactions on Aerospace and Electronic Systems*, *56*(3), 1873–1885. https://doi.org/10.1109/TAES.2019.2935962

How to cite this article: Hu, Y., & Gebre-Egziabher, D. (2026). A recursive Bayesian overbounding filter using Gaussian–Pareto distributions. *NAVIGATION*, *73*. https://doi.org/10.33012/navi.791

A | A SOLUTION TO THE CONSERVATIVE GMM APPROACH

In this section, we derive a closed-form solution to the conservative GMM optimization problem described by Equation (16), which is restated below for clarity:

$$\begin{aligned}\min_{\{\lambda_k\}_{k=1}^{n/2}} \quad & \sum_{j=1}^{m} \omega_j \| f_{\text{G-P}}(x_j) - \sum_{k=1}^{n/2} \lambda_k \mathcal{N}(x_j \,|\, \mu_k, \sigma^2) - \sum_{k=1}^{n/2} \lambda_k \mathcal{N}(x_j \,|\, -\mu_k, \sigma^2) \|^2 \\ \text{s.t.} \quad & 2\sum_{k=1}^{n/2} \lambda_k = 1, \\ & \sum_{k=1}^{n/2} \lambda_k F_{\text{Gau}}(x \,|\, \mu_k, \sigma^2)|_{x=-x_{\text{end}}} + \sum_{k=1}^{n/2} \lambda_k F_{\text{Gau}}(x \,|\, -\mu_k, \sigma^2)|_{x=-x_{\text{end}}} \geq F_{\mathbf{G\text{-}P}}(-x_{\text{end}})\end{aligned} \tag{29}$$

where n denotes the number of Gaussian mixture components and is a even number in this example, $\{\lambda_k\}_{k=1}^{n/2}$ are the optimization variables, $\{\omega_j\}_{j=1}^{m}$ represent the weighting coefficient of the curve-fitting data points $\{x_j, f_{\text{G-P}}(x_j)\}_{j=1}^{m}$, $\mathcal{N}(x \,|\, \mu_k, \sigma^2)$ denotes the PDF of the k-th Gaussian mixture component with mean μ_k and variance σ^2, $F_{\text{Gau}}(x \,|\, \mu_k, \sigma^2)$ is the CDF of the k-th Gaussian mixture component with mean μ_k and variance σ^2, and $f_{\text{G-P}}(x)$ and $F_{\mathbf{G\text{-}P}}(x)$ represent the PDF and CDF of the Gaussian–Pareto distribution.

The Karush–Kuhn–Tucker (KKT) condition can be used to solve the constrained optimization problem.

1. Stationarity:
   We set the following:

$$f(\{\lambda\}_{k=1}^{n/2}) = \sum_{j=1}^{m} \omega_j \| f_{\text{G-P}}(x_j) - \sum_{k=1}^{n/2} \lambda_k \mathcal{N}(x_j \,|\, \mu_k, \sigma^2) - \sum_{k=1}^{n/2} \lambda_k \mathcal{N}(x_j \,|\, -\mu_k, \sigma^2) \|^2 \tag{30a}$$

$$l(\{\lambda\}_{k=1}^{n/2}) = 2\sum_{k=1}^{n/2} \lambda_k - 1 \tag{30b}$$

$$\begin{aligned} h(\{\lambda\}_{k=1}^{n/2}) = F_{\mathbf{G\text{-}P}}(-x_{\text{end}}) & - \sum_{k=1}^{n/2} \lambda_k F_{\text{Gau}}(x \,|\, \mu_k, \sigma^2)|_{x=-x_{\text{end}}} \\ & - \sum_{k=1}^{n/2} \lambda_k F_{\text{Gau}}(x \,|\, -\mu_k, \sigma^2)|_{x=-x_{\text{end}}} \end{aligned} \tag{30c}$$

   Thus, we have the following:

$$\frac{\partial\{f(\{\lambda\}_{k=1}^{n/2}) + u \cdot h(\{\lambda\}_{k=1}^{n/2}) + v \cdot l(\{\lambda\}_{k=1}^{n/2})\}}{\partial \lambda_i} = 0, \quad i = 1, \cdots, \frac{n}{2} \tag{31}$$

2. Complementary slackness:

$$u \cdot h(\{\lambda\}_{k=1}^{n/2}) = 0 \tag{32}$$

3. Primal feasibility:

$$l(\{\lambda\}_{k=1}^{n/2}) = 0 \tag{33a}$$

$$h(\{\lambda\}_{k=1}^{n/2}) \leq 0 \tag{33b}$$

4. Dual feasibility:

$$u \geq 0 \tag{34}$$

Case 1: When $u > 0$, the equality must hold for the primal feasibility in Equation (33b) in order to satisfy the complementary slackness in Equation (32). Equation (31) is then as follows:

$$\frac{\partial\{f(\{\lambda\}_{k=1}^{n/2}) + v \cdot l(\{\lambda\}_{k=1}^{n/2})\}}{\partial \lambda_i} = \sum_{k=1}^{n/2}\left(\sum_{j=1}^{m} 2\omega_j \mathcal{G}(x \mid \mu_k, \mu_i, \sigma^2)\right)\lambda_k + 2v - u\mathcal{F}(-x_{\text{end}} \mid \mu_i, \sigma^2) - \sum_{j=1}^{m} 2\omega_j f_{\text{G-P}}(x_j)\mathcal{N}'(x_j \mid \mu_i, \sigma^2) = 0, \quad i = 1, \cdots, \frac{n}{2} \tag{35}$$

where:

$$\mathcal{G}(x \mid \mu_k, \mu_i, \sigma^2) = \mathcal{N}'(x \mid \mu_k, \sigma^2)\mathcal{N}'(x \mid \mu_i, \sigma^2) \tag{36a}$$

$$\mathcal{N}'(x \mid \mu_i, \sigma^2) = \mathcal{N}(x \mid \mu_i, \sigma^2) + \mathcal{N}(x \mid -\mu_i, \sigma^2) \tag{36b}$$

$$\mathcal{F}(-x_{\text{end}} \mid \mu_i, \sigma^2) = F_{\text{Gau}}(x \mid -\mu_i, \sigma^2)|_{x=-x_{\text{end}}} + F_{\text{Gau}}(x \mid \mu_i, \sigma^2)|_{x=-x_{\text{end}}} \tag{36c}$$

We define the vector $\Lambda = [\lambda_1 \quad \lambda_2 \quad \lambda_3 \quad \cdots \quad \lambda_{n/2} \quad v \quad u]^\top$. According to the KKT conditions in Equations (31)–(34), the following relationship of Λ can be established:

$$\mathbf{C}\Lambda = \mathbf{b} \tag{37}$$

where:

$$\mathbf{C} = \begin{bmatrix} \sum_{j=1}^{m} 2\omega_j \mathcal{G}(x_j \mid \mu_1, \mu_1, \sigma^2) & \sum_{j=1}^{m} 2\omega_j \mathcal{G}(x_j \mid \mu_2, \mu_1, \sigma^2) & \cdots & \sum_{j=1}^{m} 2\omega_j \mathcal{G}(x_j \mid \mu_{n/2}, \mu_1, \sigma^2) & 2 & -\mathcal{F}(-x_{\text{end}} \mid \mu_1, \sigma^2) \\ \sum_{j=1}^{m} 2\omega_j \mathcal{G}(x_j \mid \mu_1, \mu_2, \sigma^2) & \sum_{j=1}^{m} 2\omega_j \mathcal{G}(x_j \mid \mu_2, \mu_2, \sigma^2) & \cdots & \sum_{j=1}^{m} 2\omega_j \mathcal{G}(x_j \mid \mu_{n/2}, \mu_2, \sigma^2) & 2 & -\mathcal{F}(-x_{\text{end}} \mid \mu_2, \sigma^2) \\ \vdots & \vdots & \ddots & \vdots & \vdots & \vdots \\ \sum_{j=1}^{m} 2\omega_j \mathcal{G}(x_j \mid \mu_1, \mu_{n/2}, \sigma^2) & \sum_{j=1}^{m} 2\omega_j \mathcal{G}(x_j \mid \mu_2, \mu_{n/2}, \sigma^2) & \cdots & \sum_{j=1}^{m} 2\omega_j \mathcal{G}(x_j \mid \mu_{n/2}, \mu_{n/2}, \sigma^2) & 2 & -\mathcal{F}(-x_{\text{end}} \mid \mu_{n/2}, \sigma^2) \\ 2 & 2 & \cdots & 2 & 0 & 0 \\ \mathcal{F}(-x_{\text{end}} \mid \mu_1, \sigma^2) & \mathcal{F}(-x_{\text{end}} \mid \mu_2, \sigma^2) & \cdots & \mathcal{F}(-x_{\text{end}} \mid \mu_{n/2}, \sigma^2) & 0 & 0 \end{bmatrix} \tag{38a}$$

$$\mathbf{b} = \begin{bmatrix} \sum_{j=1}^{m} 2\omega_j f_{\text{G-P}}(x_j)\mathcal{N}'(x_j \mid \mu_1, \sigma^2) & \sum_{j=1}^{m} 2\omega_j f_{\text{G-P}}(x_j)\mathcal{N}'(x_j \mid \mu_2, \sigma^2) & \cdots & \sum_{j=1}^{m} 2\omega_j f_{\text{G-P}}(x_j)\mathcal{N}'(x_j \mid \mu_{n/2}, \sigma^2) & 1 & F_{\mathbf{G\text{-}P}}(-x_{\text{end}}) \end{bmatrix}^\top \tag{38b}$$

Therefore, the vector Λ can be calculated as follows:

$$\Lambda = (\mathbf{C}^\top \mathbf{C})^{-1}\mathbf{C}^\top \mathbf{b} \tag{39}$$

Then, we can determine if the computed u is greater than 0. If so, we have found the optimal solution to the GMM estimation problem. If not, we move on to the second case.

Case 2: When $u = 0$, Equation (31) is as follows:

$$\frac{\partial\{f(\{\lambda\}_{k=1}^{n/2}) + v \cdot l(\{\lambda\}_{k=1}^{n/2})\}}{\partial\lambda_i} = \sum_{k=1}^{n/2}\left(\sum_{j=1}^{m} 2\omega_j \mathcal{G}(x \mid \mu_k, \mu_i, \sigma^2)\right)\lambda_k + 2v - \sum_{j=1}^{m} 2\omega_j f_{\text{G-P}}(x_j)\mathcal{N}'(x_j \mid \mu_i, \sigma^2) = 0, \quad i = 1, \cdots, \frac{n}{2} \tag{40}$$

where:

$$\mathcal{G}(x \mid \mu_k, \mu_i, \sigma^2) = \mathcal{N}'(x \mid \mu_k, \sigma^2)\mathcal{N}'(x \mid \mu_i, \sigma^2) \tag{41a}$$

$$\mathcal{N}'(x \mid \mu_i, \sigma^2) = \mathcal{N}(x \mid \mu_i, \sigma^2) + \mathcal{N}(x \mid -\mu_i, \sigma^2) \tag{41b}$$

We define the vector $\Lambda = [\lambda_1 \quad \lambda_2 \quad \lambda_3 \quad \cdots \quad \lambda_{n/2} \quad v]^\top$. According to the KKT conditions in Equations (31)–(34), the following relationship of Λ can be established:

$$\mathbf{C}\Lambda = \mathbf{b} \tag{42}$$

where:

$$\mathbf{C} = \begin{bmatrix} \sum_{j=1}^{m} 2\omega_j \mathcal{G}(x_j \mid \mu_1, \mu_1, \sigma^2) & \sum_{j=1}^{m} 2\omega_j \mathcal{G}(x_j \mid \mu_2, \mu_1, \sigma^2) & \cdots & \sum_{j=1}^{m} 2\omega_j \mathcal{G}(x_j \mid \mu_{n/2}, \mu_1, \sigma^2) & 2 \\ \sum_{j=1}^{m} 2\omega_j \mathcal{G}(x_j \mid \mu_1, \mu_2, \sigma^2) & \sum_{j=1}^{m} 2\omega_j \mathcal{G}(x_j \mid \mu_2, \mu_2, \sigma^2) & \cdots & \sum_{j=1}^{m} 2\omega_j \mathcal{G}(x_j \mid \mu_{n/2}, \mu_2, \sigma^2) & 2 \\ \vdots & \vdots & \ddots & \vdots & \vdots \\ \sum_{j=1}^{m} 2\omega_j \mathcal{G}(x_j \mid \mu_1, \mu_{n/2}, \sigma^2) & \sum_{j=1}^{m} 2\omega_j \mathcal{G}(x_j \mid \mu_2, \mu_{n/2}, \sigma^2) & \cdots & \sum_{j=1}^{m} 2\omega_j \mathcal{G}(x_j \mid \mu_{n/2}, \mu_{n/2}, \sigma^2) & 2 \\ 2 & 2 & \cdots & 2 & 0 \end{bmatrix} \tag{43a}$$

$$\mathbf{b} = \begin{bmatrix} \sum_{j=1}^{m} 2\omega_j f_{\text{G-P}}(x_j)\mathcal{N}'(x_j \mid \mu_1, \sigma^2) & \sum_{j=1}^{m} 2\omega_j f_{\text{G-P}}(x_j)\mathcal{N}'(x_j \mid \mu_2, \sigma^2) & \cdots & \sum_{j=1}^{m} 2\omega_j f_{\text{G-P}}(x_j)\mathcal{N}'(x_j \mid \mu_{n/2}, \sigma^2) & 1 \end{bmatrix}^\top \tag{43b}$$

Therefore, the vector Λ can be calculated as follows:

$$\Lambda = (\mathbf{C}^\top\mathbf{C})^{-1}\mathbf{C}^\top\mathbf{b} \tag{44}$$

Next, we determine if the computed Λ satisfies Equation (33b); if so, we have found the optimal solution to the GMM estimation problem.